The mechanics of lubricated faults: Insights from 3-D numerical models

Andrea Bizzarri[1]

Received 13 October 2011; revised 26 March 2012; accepted 27 March 2012; published 12 May 2012.

[1] The weakening mechanisms occurring during an earthquake failure are of prominent importance in determining the resulting energy release and the seismic waves excitation. In this paper we consider the fully dynamic response of a seismogenic structure where lubrication processes take place. In particular, we numerically model the spontaneous propagation of a 3-D rupture in a fault zone where the frictional resistance is controlled by the properties of a low viscosity slurry, formed by gouge particles and fluids. This model allows for the description of the fault motion in the extreme case of vanishing effective normal stress, by considering a viscous fault response and therefore without the need to invoke, in the framework of Coulomb friction, the generation of the tensile mode of fracture. We explore the effects of the parameters controlling the resulting governing law for such a lubricated fault; the viscosity of the slurry, the roughness of the fault surfaces and the thickness of the slurry film. Our results indicate that lubricated faults produce a nearly complete stress drop (i.e., a very low residual friction coefficient; $\mu \sim 0.01$), a high fracture energy density ($E_G \sim$ few 10s of MJ/m^2) and significant slip velocities ($v_{peak} \sim$ few 10s of m/s). The resulting values of the equivalent characteristic slip-weakening distance (d_0^{eq} = 0.1–0.8 m, depending on the adopted parameters) are compatible with the seismological inferences. Moreover, in the framework of our model we found that supershear ruptures are highly favored. In the case of enlarging gap height we can have the healing of slip or even the inhibition of the rupture. Quantitative comparisons with different weakening mechanisms previously proposed in the literature, such as the exponential weakening and the frictional melting, are also discussed.

Citation: Bizzarri, A. (2012), The mechanics of lubricated faults: Insights from 3-D numerical models, *J. Geophys. Res.*, *117*, B05304, doi:10.1029/2011JB008929.

1. Introduction

[2] It is well known that the numerical modeling of the dynamics of ruptures developing on a discontinuity interface gives the chance to explore in great details the different dissipative processes that can take place during crustal earthquakes [see *Bizzarri*, 2011b, and references therein]. Friction and fracture experiments often fail to reproduce the natural conditions (in terms of both applied stresses and sliding velocity) and, moreover, the dependence of the measured friction on the imposed loading history is still unclear and further experimental efforts are needed. On the contrary, the numerical models are powerful tools to investigate faulting mechanisms in realistic conditions.

[3] The introduction of a governing law guarantees a finite energy flux at the rupture tip and makes it possible to simulate the traction evolution on the fault surface as it results from the inclusion of the various chemical and physical mechanisms which can strongly affect the traction evolution and ultimately the earthquake dynamics; the thermal weakening [*Rice*, 2006; *Bizzarri*, 2009], the pore fluid pressurization [*Lachenbruch and Sass*, 1980; *Bizzarri and Cocco*, 2006; *Brantut et al.*, 2010], the powder lubrication due to nanograins [*Han et al.*, 2010, 2011; *Reches and Lockner*, 2010], the silica gel formation [*Goldsby and Tullis*, 2002], the thermal decomposition [*Han et al.*, 2007; *Brantut et al.*, 2008], the frictional melting [e.g., *Jeffreys*, 1942; *Sibson*, 1975; *Bizzarri*, 2011a], the acoustic fluidization [*Melosh*, 1996], the normal interface vibrations [*Brune et al.*, 1993], etc. The relative importance of these different dissipative mechanisms can depend on the presence of fluids in the seismic structure, its hydraulic properties and its maturity, the level of development of the fault fabric, the rock type, etc. Formally, the presence of friction-induced melts is not a direct evidence of lubrication by itself, and, what is more, the efficiency of melt lubrication [*Spray*, 1993] has been questioned [*Scholz*, 2002; *Koizumi et al.*,

[1]Istituto Nazionale di Geofisica e Vulcanologia, Sezione di Bologna, Bologna, Italy.

Corresponding author: A. Bizzarri, Istituto Nazionale di Geofisica e Vulcanologia, Sezione di Bologna, Via Donato Creti 12, I-40128 Bologna, Italy. (bizzarri@bo.ingv.it)

Copyright 2012 by the American Geophysical Union.
0148-0227/12/2011JB008929

2004]. Recently, the thermal runaway has been reproduced in laboratory friction experiments, performed at relatively low normal stress [*De Paola et al.*, 2011, and references therein], indicating that the fault strength can drop dramatically and can induce very large dynamic stress drops. Laboratory evidences suggest that, at seismic slip rates ($\sim$1 m/s or more), simulated faults can be extraordinarily weak or slippery [e.g., *Han et al.*, 2011].

[4] In addition to its inherent relevance in the mechanics of faulting — the complex wave forms at high frequency are controlled by the microscopic processes occurring on the fault zone —, the study of friction, lubrication and wear (i.e., of the so-called tribology) [*Great Britain Department of Education and Science*, 1966] has an enormous importance in modern-day civilization, because it affects performance and life of all mechanical systems and because it provides reliability, precision and accuracy of many of them [*Szeri*, 2011].

[5] The frictional resistance acting on a seismogenic structure is analytically described by the a governing model for faults, such as the slip-dependent laws, the rate- and state-dependent laws with memory, etc. (see *Bizzarri* [2011b] for a compendious review), which represents in an average, macroscopic sense, the behavior at the microscopic asperity contacts level.

[6] The focus of this paper is on lubrication. Sometimes [e.g., *Di Toro et al.*, 2011] the term fault lubrication is used to generally indicate a significant, often dramatic, decrease of the friction coefficient (up to one order of magnitude), without reference to the specific weakening mechanism involved. Usually, the introduction of a lubricant between two sliding surfaces is used to lower the frictional resistance and to reduce (or even prevent) wear. Depending on the thickness of the lubricant, we can have boundary, or thin film, lubrication — during which the frictional coefficient μ decreases significantly with respect to the unlubricated regime — or thick film lubrication — where μ linearly increases with the dimensionless Sommerfeld number (also named bearing characteristic number):

$$So \equiv \frac{p_{\mathrm{res}} + p_{\mathrm{lub}}}{\sigma_n} \tag{1}$$

i.e., following the Petroff's law [*Sommerfeld*, 1950]. In equation (1) p_{res} is the reference pore fluid pressure of the reservoir in the far-field, p_{lub} is the lubricant pressure and σ_n is the normal stress. (Incidentally, we recall here that if σ_n expresses the lithostatic pressure, then *So* is the so-called pore fluid pressure number λ.) A qualitative description of these different regimes (thin and thick film lubrication) can be found in the Stribek curve of *Spikes* [1997, Figure 1].

2. Physical Model

[7] In this study we consider a 3-D rupture which spreads over a planar, vertical, strike-slip fault parallel to the $x_2 = 0$ plane. In the $Ox_1x_2x_3$ Cartesian coordinate system x_1 is the strike coordinate and x_3 is the depth; $x_3 = 0$ is the free surface, where the free-of-traction condition is imposed. The geometry of the model is the same as that of *Bizzarri* [2011b, Figure 14a]. To simplify the notation in the remainder of the paper we will omit the explicit indication of the dependence of the dynamic variables on the spatial and temporal coordinates (a generic variable V is in fact $V(x_1, x_3, t)$ and so on).

[8] We assume that the fault contains some fluids (basically water) and gouge. Indeed, there are several indications that the fault gouge is present in major faults, such as the San Andreas fault [*Wu et al.*, 1975]. In fault structures characterized by the presence of ample aqueous fluids they can be squeezed out of the slipping zone, where the deformation is concentrated, due to the thermal pressurization phenomenon [e.g., *Lachenbruch*, 1980; *Bizzarri and Cocco*, 2006; *Rice*, 2006, and references cited therein]. *Segall and Rice* [2006] show that the thermal pressurization is active only in a late stage of the slow earthquake nucleation process, namely, when the sliding speeds are of the order of 1 mm/s or more. Once the fluid content of the fault structure is reducing, we hypothesize that the gouge, rich of particles, forms the slurry with the remaining water. Namely, the slurry is a thick suspension of solids in the fluids, i.e., a mixture of water and wear products, generated as a consequence of gouge refinement, abrasion, and pulverization within the slipping zone thickness. The slurry basically represents the lubricant material referenced above. We also mention that the fault gouge at depth can be compacted or solidified to form cataclasite, which may require some process to form the slurry which acts as a viscous fluid; in the present treatment we assume that slurry can be formed with remaining fluids.

[9] Once the slurry has been formed, due to its high viscosity (the slurry is more viscous than the pure water), the thermally-activated pore fluid pressurization is negligible with respect to the lubrication or it is no longer possible; therefore the lubrication effects are paramount.

[10] In this paper we assume that the fault under study has already formed the slurry, for instance in previous earthquake failures; at $t = 0$ the lubrication is active, due to the presence of the slurry film. We will denote with $2w$ the thickness of this thin gap which separates the two sliding surfaces defining the fault structure. Namely, $2w$ is physically defined as the thickness which is much shorter than the on fault-length over which the fluid pressure changes significantly.

[11] The behavior of the slurry is described by the solution of the Navier-Stokes equations for each node of the fault, coupled with the continuity equation for the fluid. In this paper we follow the formulation of *Brodsky and Kanamori* [2001], also employed by *Ma et al.* [2003]. First of all, let introduce the effective normal stress, which in the framework of Coulomb friction is expressed as

$$\sigma_n^{eff} = \sigma_n - p_{res} - p_{lub}. \tag{2}$$

[12] To better understand the effects on rupture dynamics of the lubrication we also neglect possible differences in the material properties of the two sides of the fault so that we have no variations in σ_n. Moreover, we emphasize that the flow characteristic of the slurry can change widely as a consequence of the size of the suspended solid particles, which can vary from fine colloidal particles to sedimentable coarse particles, of the particle size distribution, of their shape and surface properties and of their concentration within the liquid. Indeed, the dynamic viscosity of the of the slurry (η) can change through time because of pulverization and further wear; in this case the volume fraction ϕ of the

solid particles will change and it would lead to a time variation of η of the type [e.g., *Guth and Simha*, 1936] $\eta = \eta_{liquid}(1 + 2.5\phi + 14.1\phi^2)$, where η_{liquid} is the dynamic viscosity of the liquid (or water). (Incidentally, we report here that a simplified relation, $\eta = \eta_{liquid}(1 + 2.5\phi)$, was due to A. Einstein [*Zolotarev et al.*, 1966].) Finally, we ignore the dependence of η (basically through possible dependencies in η_{liquid}) on the pressure and on the temperature, by making the assumption of an isoviscous slurry. Of course, this can be regarded as a potential limitation of the model; at the present state we do not have a sufficiently robust model to physically describe the chemical and physical properties (and their temporal changes) of the slurry. The isovisocus slurry have to be regarded as a first-order approximation of the true behavior of the slurry.

[13] Analytically, we express the fault traction τ, which in turn controls the seismic motion, as follows (see also equation (27) in *Brodsky and Kanamori* [2001]):

$$\tau = \begin{cases} \mu_u \sigma_n^{\text{eff}} + \dfrac{\langle 2w \rangle}{u} p_{\text{lub}} = \mu_u \sigma_{n_0} - \left(\mu_u - \dfrac{\langle 2w \rangle}{u} \right) p_{\text{lub}} & , So < 1 \\ \dfrac{\langle 2w \rangle}{u} p_{\text{lub}} & , So \geq 1 \end{cases} \tag{3}$$

where μ_u is the static level of friction ($\tau_u \equiv \mu_u \sigma_n^{eff}$ is the upper yield stress), $\sigma_{n_0} \equiv \sigma_n(t = 0) \equiv \sigma_n - p_{res}$ ($= \sigma_{n_0}^{\text{eff}} \equiv \sigma_n^{eff}(t = 0)$) and *So* has been defined above (see equation (1)).

[14] The governing model (3) basically states that at the very low Sommerfeld numbers the fault obeys a Coulomb-based rheology, in which the conventional notion of solid friction, directly proportional to the normal stress, is appropriate. This framework, in which the coefficient of friction (μ) is reasonably independent on the applied load, is no longer valid when σ_n^{eff} approaches zero (or equivalently when *So* approaches 1) and for large values of *So*; in this situation the solid-solid friction is changed into a viscous behavior. In this case we enter the so-called hydrodynamic lubrication [*Szeri*, 2011].

[15] We emphasize here that the present model, because of the presence of the slurry which is assumed to be already present on the fault zone since $t = 0$, prescribes a transition to a fully lubricated regime depending on the value of *So*. The comparison between the present model and the viscous behavior of a continuous layer of an high viscosity molten material [*Bizzarri*, 2011a] is discussed in Appendix B.

[16] In equation (3) u is the magnitude of the (local, i.e., in (x_1, x_3) and at time t) fault slip and the operator <·> indicates the average value (over the whole extension of the fault and at time t) of the thickness of the slurry film (gap height). Indeed, we know that the tribological surfaces are characterized by a topology which deviates from a plane [e.g., *Power and Tullis*, 1991; *Scholz*, 2002] and the gap height can be spatially variable even within the same fault structure [*Rathbun and Marone*, 2010]. This would require the specification of the exact topology of the thickness of the slurry, which poses a practical problem, since it is difficult to obtain a statistically representative topology of asperities and gaps of sliding surfaces [*Spikes*, 1997]. If we assume that the gap height is constant through time, then $\langle 2w \rangle = \langle 2w_0 \rangle$ is an average, representative value for the whole spatial extension of the fault. If we assume that $\langle 2w \rangle$ evolves through time (see equations (6) and (7)), then the initial value of $2w$ is spatially uniform, but the spatial heterogeneity of u will introduce a spatial heterogeneity in the thickness of the slurry film at each time.

[17] The lubrication pressure p_{lub} appearing in the constitutive model (3) is the solution of the following equation:

$$\langle 2w \rangle^3 p_{\text{lub}} - 6\eta\, r\, u^2\, v = 0 \tag{4}$$

where the dimensionless number r quantifies the roughness of the fault, assumed to be constant through time [*Brodsky and Kanamori*, 2001] and v is the time derivative of u.

[18] Plenty of high-velocity studies [*Tsutsumi and Shimamoto*, 1997; *Tullis and Goldsby*, 2003a, 2003b; *Prakash and Yuan*, 2004; *Hirose and Shimamoto*, 2005; *Beeler et al.*, 2008] indicate an extreme velocity-weakening response of simulated faults. Purely velocity-dependent friction models can lead to unphysical phenomena or mathematically ill-posed problems, in that they are very unstable at low values of the fault slip velocity, both during the passage of the rupture front and during the possible slip arrest phase [e.g., *Cochard and Madariaga*, 1994; *Madariaga and Cochard*, 1994]. Indeed, the model proposed here is a slip- and velocity-dependent model, like that proposed by *Sone and Shimamoto* [2009] and recently adopted in numerical models of seismic fault by *Bizzarri* [2010b]. This analogy is discussed in detail in Appendix B.

[19] The formulation of equation (3) assumes that the fluid flow is laminar, i.e., that the following condition is met:

$$Re \equiv \frac{\langle 2w \rangle \rho\, v}{\eta} \leq 2 \times 10^3 \tag{5}$$

where Re is the Reynolds number and ρ is the cubic mass density of the slurry. This condition is satisfied for typical values of the parameters and for the velocities resulting from all the numerical experiments presented in the present paper.

[20] In equations (3) and (4) we allow for a possible elastic deformation of the walls, resulting in a temporal variation of the average gap height; this situation formally defines the elastohydrodynamic lubrication (EHL). Following *Brodsky and Kanamori* [2001, see their equation (17)] we will consider the following relation, expressing that the gap height is given by the initial gap and an average elastic displacement:

$$\langle 2w \rangle = \langle 2w_0 \rangle + \frac{p_{\text{lub}}}{E} u \tag{6}$$

being $\langle 2w_0 \rangle$ the initial (i.e., at $t = 0$) value of the average thickness of the slurry film $\langle 2w \rangle$ and E the Young's modulus (which defines the stiffness of the elastic material). The explicit time dependence of the gap height on the cumulative slip stated by equation (6) is also in agreement indications from faults in mines, at outcrops and in laboratory specimens that wear processes cause the slipping zone (and thus the slurry film) to enlarge [*Hull*, 1988; *Marrett and Allmendinger*, 1990]. The analytical solution of equation (4) when $\langle 2w \rangle$ obeys equation (6) is derived in Appendix A.

[21] A simplified version of equation (6) is that proposed by *Power et al.* [1988], which reads

$$\langle 2w \rangle = \langle 2w_0 \rangle + 2K u \tag{7}$$

Table 1. Summary of the Constitutive Equations for the Lubrication Model Considered in the Paper[a]

Evolution of the (Average) Gap Height $\langle 2w \rangle$	Constitutive Equations
Not specified (i.e., general case)	
Lubrication pressure	Expressed by the solution of equation (4): $\langle 2w \rangle^3 p_{lub} - 6\,\eta\, r\, u^2\, v = 0$
Frictional resistance	$\begin{cases} \mu_u \sigma_n^{eff} + \frac{\langle 2w \rangle}{u} p_{lub} = \mu_u \sigma_{n_0} - \left(\mu_u - \frac{\langle 2w \rangle}{u} \right) p_{lub} & ,So < 1 \\ \frac{\langle 2w \rangle}{u} p_{lub} & ,So \geq 1 \end{cases}$
Constant $\langle 2w \rangle = \langle 2w_0 \rangle$, $\forall t \geq 0$	
Lubrication pressure	$\frac{6\,\eta\, r}{\langle 2w_0 \rangle^3} u^2\, v$
Frictional resistance	$\begin{cases} \mu_u \sigma_{n_0} - \frac{6\,\eta\, r\, \mu_u}{\langle 2w_0 \rangle^3} u^2\, v + \frac{6\,\eta\, r}{\langle 2w_0 \rangle^2} u\, v & ,So < 1 \\ \frac{6\,\eta\, r}{\langle 2w_0 \rangle^2} u\, v & ,So \geq 1 \end{cases}$
Non-linear increase $\langle 2w \rangle = \langle 2w_0 \rangle + \frac{p_{lub}}{E} u$ (equation (6); E is the Young's modulus)	
Lubrication pressure	$p_{lub}^{(\mathrm{IV})} = -\frac{3}{2} a + l + n$ where the constants a, l and n are defined in equation (A2)
Frictional resistance	$\begin{cases} \mu_u \sigma_{n_0} - \left(\mu_u - \frac{\langle 2w_0 \rangle}{u} \right) p_{lub}^{(\mathrm{IV})} + \frac{p_{lub}^{(\mathrm{IV})\,2}}{E} & ,So < 1 \\ \frac{\langle 2w_0 \rangle}{u} p_{lub}^{(\mathrm{IV})} + \frac{p_{lub}^{(\mathrm{IV})\,2}}{E} & ,So \geq 1 \end{cases}$
Linear increase $\langle 2w \rangle = \langle 2w_0 \rangle + 2\,K\,u$ (equation (7); K is a constant)	
Lubrication pressure	$\frac{6\,\eta\, r}{(\langle 2w_0 \rangle + 2K\,u)^3} u^2\, v$
Frictional resistance	$\begin{cases} \mu_u \sigma_{n_0} - \left(\mu_u - \frac{\langle 2w_0 \rangle}{u} \right) \frac{6\,\eta\, r}{(\langle 2w_0 \rangle + 2K\,u)^2} u\, v & ,So < 1 \\ \frac{6\,\eta\, r}{(\langle 2w_0 \rangle + 2K\,u)^2} u\, v & ,So \geq 1 \end{cases}$

[a]Here σ_n^{eff} is the effective normal stress (see equation (2)), $\sigma_{n_0} \equiv \sigma_n - p_{res}$ and So is the Sommerfeld number (see equation (1)).

where the constant $K \in [0.001, 0.1]$ furnishes a linear dependence on the cumulated slip [see also *Bizzarri*, 2010e].

[22] Following the model of *Brodsky and Kanamori* [2001] we have that the elastic deformation of the walls due to lubrication cannot be neglected if, in a given fault node and at a given time, the following condition is realized:

$$u > L_{\mathrm{lub}_c} \equiv 2\langle 2w_0 \rangle \left(\frac{\langle 2w_0 \rangle E}{6\eta\, r\, v} \right)^{\frac{1}{3}} \tag{8}$$

in which L_{lub_c} is a critical lubrication length [see also *Ma et al.*, 2003], which basically defines the length at which the elastic deformation is comparable to the initial gap height.

[23] In the special case of a temporally constant thickness of the slurry film ($\langle 2w \rangle = \langle 2w_0 \rangle$, $\forall t \geq 0$), from equation (4) we simply have

$$p_{\mathrm{lub}} = \frac{6\,\eta\, r}{\langle 2w_0 \rangle^3} u^2\, v \tag{9}$$

and therefore the constitutive model (3) reduces to

$$\tau = \begin{cases} \mu_u \sigma_{n_0} - \frac{6\,\eta\, r\, \mu_u}{\langle 2w_0 \rangle^3} u^2\, v + \frac{6\,\eta\, r}{\langle 2w_0 \rangle^2} u\, v & ,\, So < 1 \\ \frac{6\,\eta\, r}{\langle 2w_0 \rangle^2} u\, v & ,\, So \geq 1 \end{cases} \tag{10}$$

On the other hand, when the evolution of $\langle 2w \rangle$ follows equation (7) we can write

$$p_{\mathrm{lub}} = \frac{6\,\eta\, r}{(\langle 2w_0 \rangle + 2K\,u)^3} u^2\, v \tag{11}$$

and the counterpart of equation (10) is straightforward. For completeness, the equations for the lubrication pressure (p_{lub}) and for the frictional resistance (τ) for the different evolutions of the average thickness of the slurry film are compendiously reported in Table 1.

3. Quantitative Evaluations for Prescribed Slip Velocity Time Histories

[24] Before analyzing the behavior of a rupture spontaneously developing in a lubricated seismogenic structure (as done in sections 4 and 5) we will consider here some general aspects of the mechanical lubrication model by assuming, in a generic fault node, a prescribed slip velocity time history. Namely, this is not a kinematic modeling of a fault, in that the traction evolution is not retrieved by solving the equations of motion, but it is simply computed from the given source time function. Nevertheless, this kind of preliminary

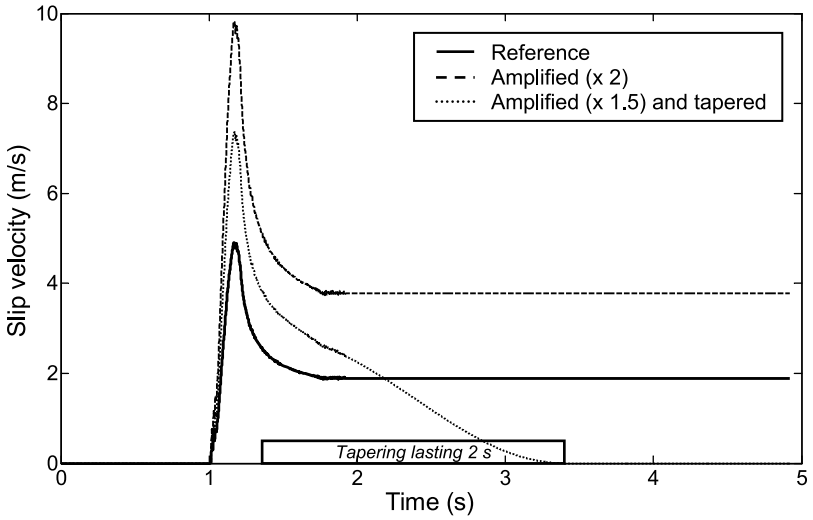

Figure 1. Time evolution of the fault slip velocity assumed to quantitatively evaluate the effects of the lubrication model. Black line is a reference, representative time history of v, dashed line is the reference time series with doubled values, and dotted line is the reference v multiplied by a coefficient equal to 1.5 and tapered to zero with a cosine function (see section 3 for details). The time window where the tapering is applied is also indicated in the plot.

study is interesting, because it gives us the possibility to evaluate the general effects of the parameters of the model.

[25] We hypothesize that the prior-assigned v is that reported in Figure 1; this time series represents a typical temporal evolution of the fault slip velocity for an earthquake failure. In particular, we consider three cases, the first is representative of a crack-like solution, in which the final slip velocity is nonzero (solid line); namely, this time series comes from a spontaneous supershear dynamic rupture with homogeneous conditions. This detail is unimportant; indeed, we know that supershear ruptures predict a different frequency content in the time evolution of the fault slip velocity with respect to that of subshear ones [*Bizzarri and Spudich*, 2008], but the calculation of the resulting p_{lub} is not sensitive to these spectral differences. The second case of slip velocity time history we consider is identical to the previous one, but now we double the values of v (dashed line) and the third case pertains to a pulse-like solution (dotted line). The latter is obtained from the reference case (solid line), by applying a multiplier factor of 1.5 and by applying a cosine-tapering at the time t = 1.4 s (in order to preserve the peak of v and its spectral content) and lasting 2 s. This time series represents a situation in which the healing of slip occurs, so that the fault slip velocity has a compact support. (We are not interested here in the study of the specific mechanism causing this cessation of slip; this has been the subject of different studies [e.g., *Bizzarri*, 2010c, and references therein].)

[26] For all the three cases the fault slip u is obtained by exploiting the first-order, forward finite difference approximation: $u^{(m+1)} = u^{(m)} + v^{(m+1)}\,\Delta t$, where the constant Δt is the time step and the superscript m denotes the time level $t_m = m\,\Delta t$.

[27] We will consider three parameters which control the governing model (3); the dynamic viscosity of the slurry (η), the size of the gap height ($\langle\, 2w \,\rangle$) and the static level of the friction coefficient (μ_u). In the simplest case of a constant $\langle\, 2w \,\rangle$ we plot in Figures 2–4 the various quantities of the lubrication model for representative values of η (Figure 2), $\langle\, 2w_0 \,\rangle$ (Figure 3) and μ_u (Figure 4).

[28] Overall, we can remark that, as expected from equation (3), the lubrication pressure and thus the fault traction are related to the slip velocity histories; in particular, the cessation of slip causes a diminution (toward zero) of p_{lub} after its peak (Figures 2a, 3a, and 4a). This might cause So to decrease and become again smaller than 1, so that the fault point come back again to the Coulomb regime. Physically, this tells us that the sliding velocity is crucial to determine the effectiveness of the lubrication process. We note that Figures 2f, 3f, and 4f reproduce the qualitative behavior of the Stribek curve of *Spikes* [1997, Figure 1] (see also *Brodsky and Kanamori* [2001, Figure 7]). As expected, the transition to a fully lubricated regime (marked in the plots by a vertical, dashed, black line) occurs at So = 1, when the effective normal stress vanishes.

[29] Moreover, the values of v (and the correspondent cumulated fault slip) control the duration of the breakdown processes (during which the stress is released and τ decreases significantly; Figures 2d, 3d, and 4d), as well as the so-called equivalent characteristic slip-weakening distance (d_0^{eq}) [*Bizzarri and Cocco*, 2003] (see Figures 2e, 3e, and 4e). As long as v increases (which can be physically associated to an increasing degree of instability of the rupture) d_0^{eq} decreases. We also remark that the large values of d_0^{eq} (of the order of 2 m or more) which are predicted in some configurations do not contrast with laboratory inferences [e.g., *De Paola et al.*, 2011] having similar loading velocity values.

[30] A prominent role is played by the gap height. Indeed, it is interesting to emphasize here that for large values of the thickness of the slurry film the breakdown processes are slow and consequently d_0^{eq} cannot be attained in the considered time window. We also remark that a decrease of a factor of 2 in $\langle\, 2w_0 \,\rangle$ will cause variations in p_{lub} that are 1.5

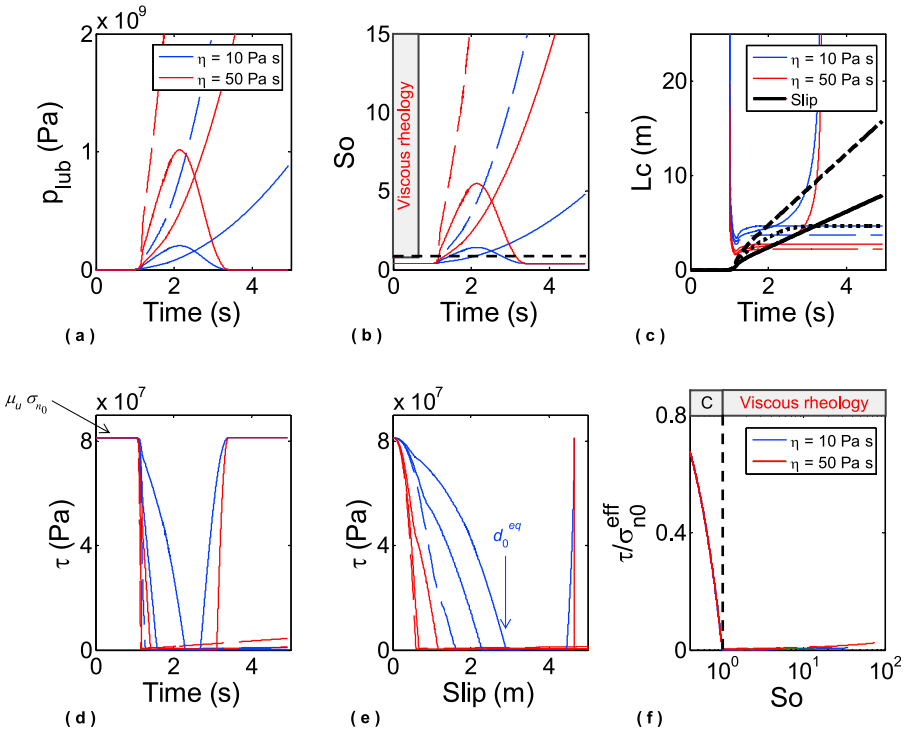

Figure 2. Results obtained by assuming the time evolution of v as in Figure 1; the fault slip u is retrieved from v by numerical integration. Here we vary the dynamic viscosity of the slurry (η), as indicated in the legends; all the other parameters are those tabulated in Table 2. For simplicity, the gap height is assumed to be constant through time (i.e., $\langle 2w \rangle = \langle 2w_0 \rangle$, $\forall t \geq 0$). (a) Time evolution of the lubrication pressure (as given by equation (9)). (b) Time evolution of the Sommerfeld number (defined in equation (1)). (c) Time evolution of the critical lubrication length (equation (8)), with the superimposition of the slip (black curves). (d) Time evolution of the traction (τ is given as in equation (10)). (e) Slip-weakening curve with the indication of the equivalent characteristic slip-weakening distance d_0^{eq} (shown only for one case, for graphical purposes). (f) Ratio between τ as shown in Figure 2d and the initial effective normal stress $\sigma_{n_0}^{eff} = \sigma_n - p_{res} - p_{lub_0}$ as a function of *So*. Note the semi-logarithmic scale in Figure 2f.

times those resulting by considering an increase of a factor of 5 in η.

[31] An important outcome is that the slip can exceed the critical lubrication length (see Figures 2c, 3c, and 4c); in this case the assumption of a constant average gap height is no longer adequate and therefore we need to consider the more complete solution for p_{lub}, as it arises from the coupled equations (4) and (6). We recall that the general solution for the lubrication pressure is derived in Appendix A.

[32] To quantitatively evaluate the effects of a variable thickness of the slurry film we compare in Figure 5 the predictions from models with constant and variable $\langle 2w \rangle$ (blue and red curves, respectively). In the latter case $\langle 2w \rangle$ evolves accordingly to equation (6) and the lubrication pressure is formally $p_{lub}^{(IV)}$ in equation (A1). The corresponding time evolution of $\langle 2w \rangle$, for the reference slip velocity history (untapered and unamplified; solid curve in Figure 1) is reported in the inset panel of Figure 5f. We can clearly see that the evolution of the traction is rather different in the two cases (see Figures 5d and 5e); the weakening becomes more close to an exponential decrease and the identification of d_0^{eq} is not straightforward, as in the case of a constant gap height. By the way, the exponential weakening has been postulated or inferred in many theoretical models [*Lachenbruch*, 1980; *Mase and Smith*, 1987; *Matsu'ura et al.*, 1992; *Bizzarri and Cocco*, 2006; *Rice*, 2006; *Bizzarri*, 2010b] and in laboratory friction experiments [*Wibberley and Shimamoto*, 2005; *Sone and Shimamoto*, 2009; *De Paola et al.*, 2011]. We will discuss more closely this issue in Appendix B.

[33] From this preliminary analysis it emerges that even before the condition (8) is verified, the variations of $\langle 2w \rangle$ markedly alter the behavior of the system, for the given slip and velocity histories. In particular, $p_{lub}^{(IV)}$ is limited so that the system does not enter in the viscous regime, for the adopted parameters. We emphasize that we can obtain a transition to the fully lubricated regime also for a time variable gap height; in Figure 6 we plot the solution for two cases where $\langle 2w \rangle$ varies and where a different value of η or $\langle 2w_0 \rangle$ was assumed (for simplicity we plot the solution pertaining only to the reference fault slip velocity history). In these configurations the progressive enlargement of $\langle 2w \rangle$ still affects the lubrication pressure, which does not increase indefinitely, as in the case of constant gap height (see Figures 2a, 3a and 4a, solid lines). However, the values of η or $\langle 2w_0 \rangle$ guarantee *So* to exceed 1, so that the viscous regime is reached (Figure 6a). Correspondently, the traction evolution exhibits again large stress drops (Figure 6b),

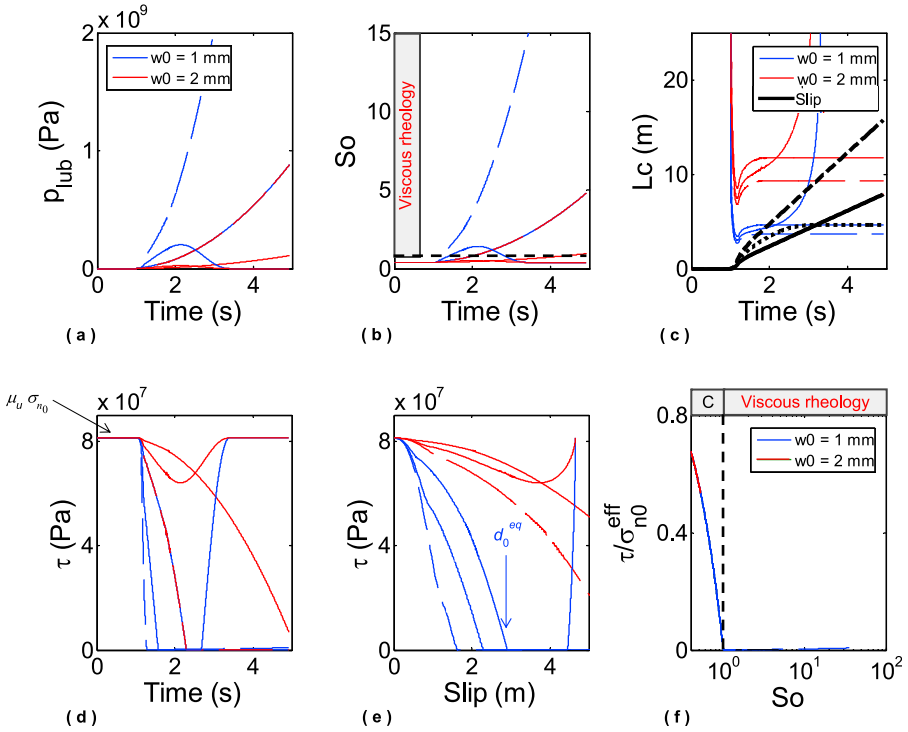

Figure 3. The same as in Figure 2, but now we change the value of the average thickness of the slurry film ($\langle 2w_0 \rangle$).

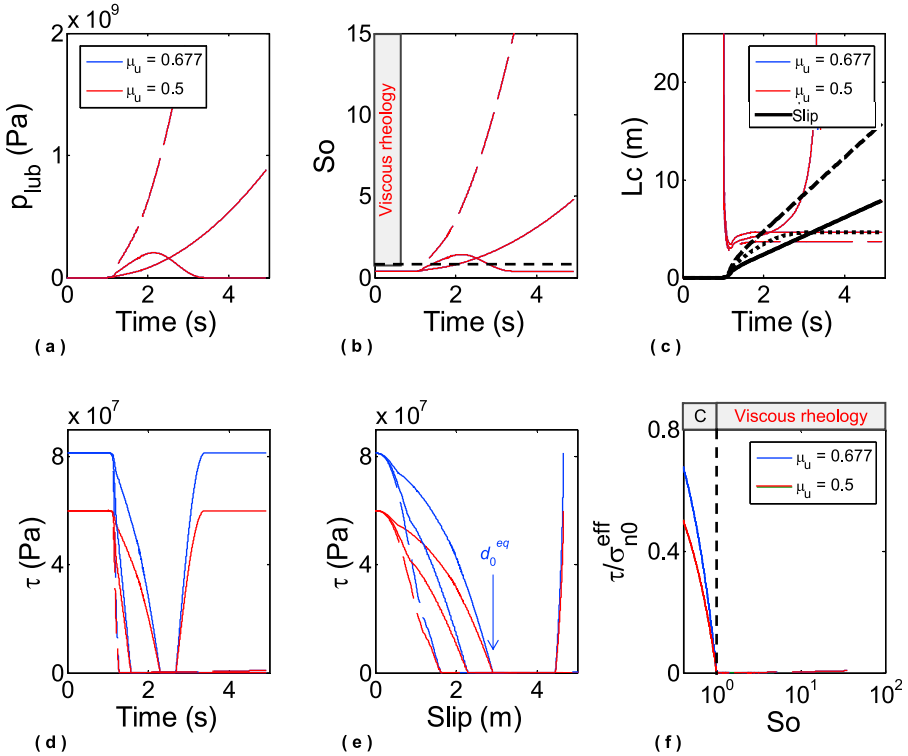

Figure 4. The same as in Figure 2, but now we change the value of the static level of the friction coefficient (μ_u), by considering two representative values of the coefficient of internal friction [*Jaeger and Cook*, 1979]. Note that since the lubrication pressure, the Sommerfeld number and the critical lubrication length do not explicitly depend on μ_u; Figures 4a–4c are identical for the two different values of μ_u.

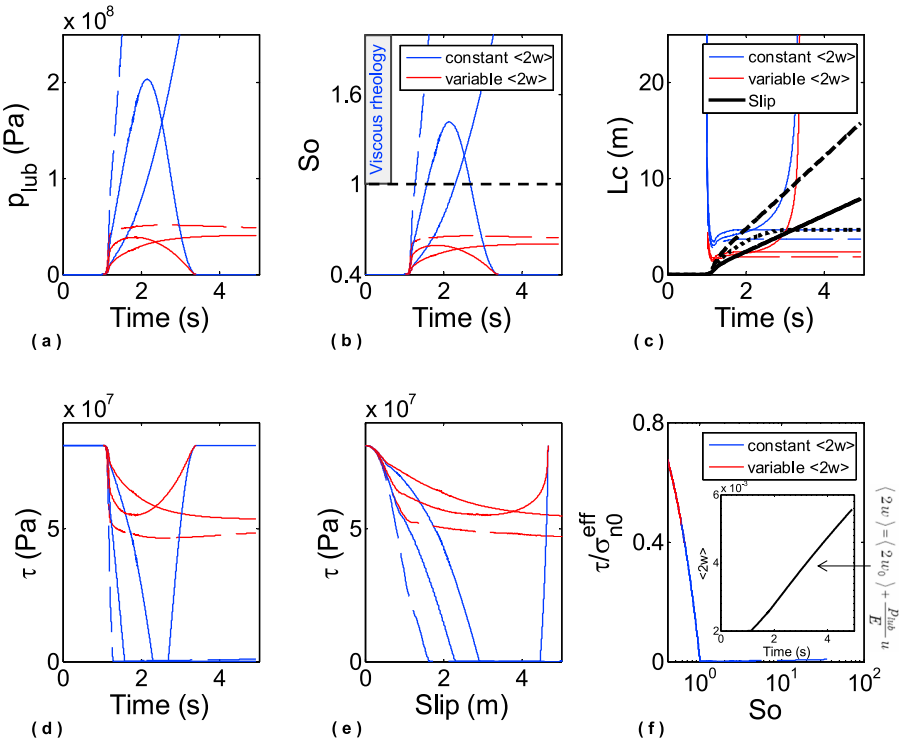

Figure 5. The same as in Figure 2, but now the comparison is between constant and variable gap height models (blue and red curves, respectively); in the latter cases the lubrication pressure is $p_{lub}^{(IV)}$ in equation (A1) and the evolution of $\langle 2w \rangle$ is that of equation (6). All the parameters are those listed in Table 2. In the inset of panel (f) we plot the evolution of the average thickness of the slurry film corresponding to the lubrication pressure in the case of the reference (i.e., untapered and unamplified; solid curve in Figure 1) fault slip velocity history. We can clearly see that $\langle 2w \rangle$, except for the initial stage of the rupture, linearly increases with time.

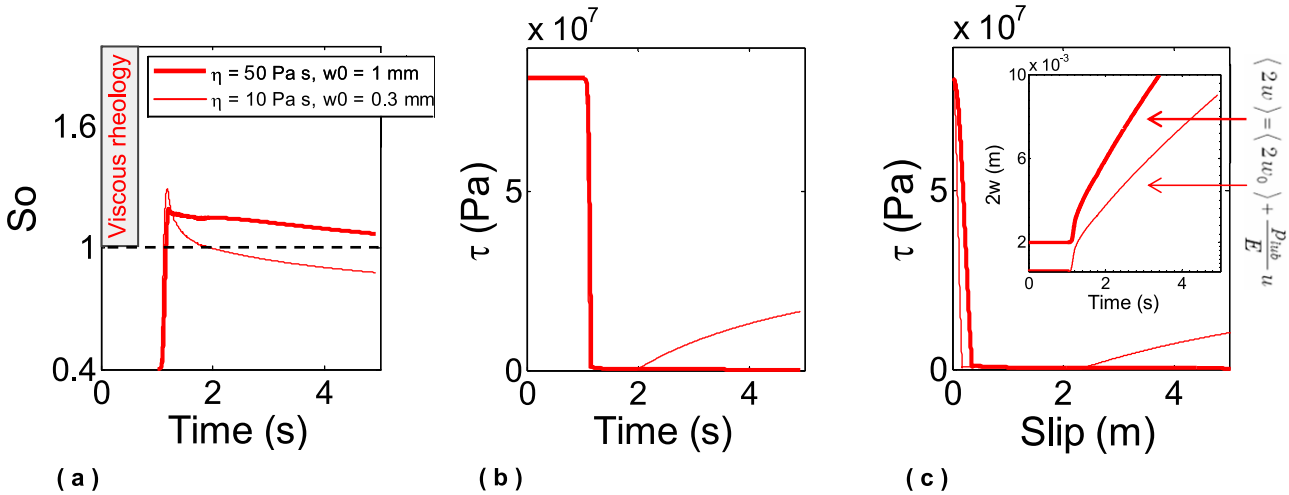

Figure 6. Evolution of the system when $\langle 2w \rangle$ varies accordingly to equation (6), for the reference fault slip velocity history and for different values of η and $\langle 2w_0 \rangle$. (a) Time evolution of the Sommerfeld number. (b) Time evolution of traction. (c) Slip-weakening curve, with inset reporting the evolution of the gap height. With the adopted parameters $p_{lub}^{(IV)}$ allows for a transition to the fully lubricated regime.

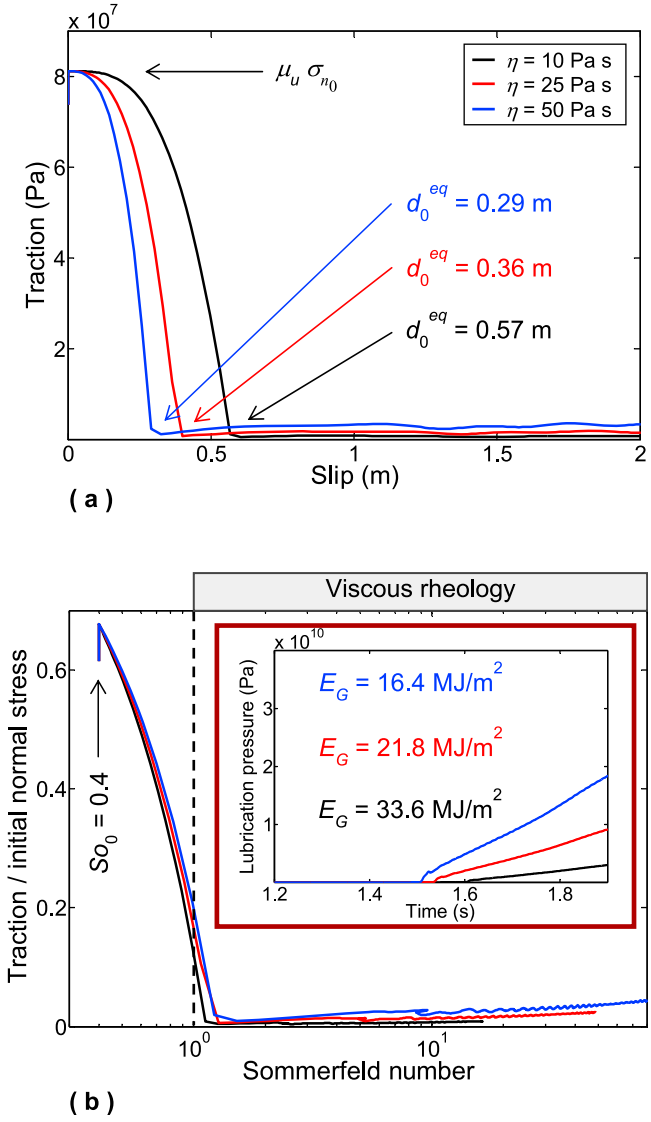

Figure 7. Results for spontaneous models with constant average thickness of the slurry film. The reference parameters are those reported in Table 2 and we vary the dynamic viscosity of the slurry η (values reported in the legend of Figure 7a). The solutions refer to a fault receiver located at the hypocentral depth and at a distance of 6 km from the hypocenter. This distance ensures that the effects of the imposed nucleation are unimportant. (a) Traction versus slip curve, with the values of the equivalent characteristic slip-weakening distance (d_0^{eq}), estimated as the fault slip developed up to the first minimum of fault traction. (b) Stribek curve, with inset panel reporting the time evolution of the lubrication pressure resulting from the models and the resulting fracture energy densities. The small oscillations of the traction after the completion of the stress release are purely numerical.

without the exponential weakening (Figure 6c), as in the configurations with constant $\langle\, 2w_0 \,\rangle$ (see Figures 2e, 3e and 4e, solid lines).

4. Fully Spontaneous Modeling of Lubricated Faults: Constant Thickness of the Slurry Film

[34] In the present section we will focus on the spontaneous (i.e., without prior-imposed rupture speed) propagation of a rupture obeying the lubrication model described in section 2, under the special assumption of a temporally constant thickness of the slurry film. We will consider the more general case where the gap height evolves through time in section 5. In the spontaneous models presented here the slip velocity time history is not prior-assigned, as in the previous analysis, but it is itself a part of the solution of the problem.

[35] The elastodynamic problem for our 3-D fault geometry is solved numerically by using a 2nd-order accurate, OpenMP-parallelized, finite-difference, conventional-grid (FDCG) code [*Bizzarri and Cocco*, 2005; *Bizzarri*, 2009]. We assume that the initial stress τ_0 is homogeneous over the fault surface, which is initially at rest (i.e., $v_0 = 0$). The governing model assumed here (equation (10)) does not allow for a description of the hardening stage of the fault, unlike other friction models [e.g., *Ruina*, 1983; *Sone and Shimamoto*, 2009]. As thoroughly discussed in *Bizzarri* [2010a], to simulate the ongoing rupture propagation it is necessary to initially impose the nucleation, which is obtained by initially forcing the rupture to enlarge at a constant rupture speed (which equals to 2.4 km/s in our simulations). Also the breakdown stress drop is imposed in the nucleation patch; $\Delta\tau_b = \tau_u - \tau_f = 57.24$ MPa. The dynamic load originating from this forced rupture guarantees a spontaneous propagation outside the nucleation patch, where the lubrication model fully controls the traction evolution.

[36] We present here a selection of the results from numerical simulations obtained by adopting different parameters; in Figure 7 we vary only the value of the dynamic viscosity of the slurry (η), in Figure 8 we vary only the average gap height ($\langle\, 2w_0 \,\rangle$) and in Figure 9 we vary only the roughness parameter (r). All the ruptures are supershear, in that their rupture velocity exceeds the S wave speed. The adopted parameters are tabulated in Table 2.

[37] We can notice several systematic trends, which confirm the previous findings obtained with a prior-assigned slip velocity time history. *i*) The breakdown process is less abrupt as long as η and r decrease and as long as $\langle\, 2w_0 \,\rangle$ increases; correspondingly the initial roll-off of the traction is longer (see Figures 7a, 8a, and 9a). *ii*) d_0^{eq} increases for decreasing η and r and for increasing $\langle\, 2w_0 \,\rangle$ and *iii*) the opposite holds for the value of the traction attained when $u = d_0^{eq}$ (i.e., τ_f^{eq}; see again Figures 7a, 8a, and 9a). We remark that the changes in τ_f^{eq} are quite small; we obtain values between 1 and 1.2 MPa. *iv*) In agreement with equation (9), the lubrication pressure p_{lub} increases when η and r increase and when $\langle\, 2w_0 \,\rangle$ decreases (see inset in Figures 7b, 8b, and 9b). *v*) In the fully lubricated regime (i.e., when $So \geq 1$) the rate of increase of the traction τ becomes more significant as η and r increase and when $\langle\, 2w_0 \,\rangle$ decreases (see the Stribek curve in Figures 7b, 8b, and 9b).

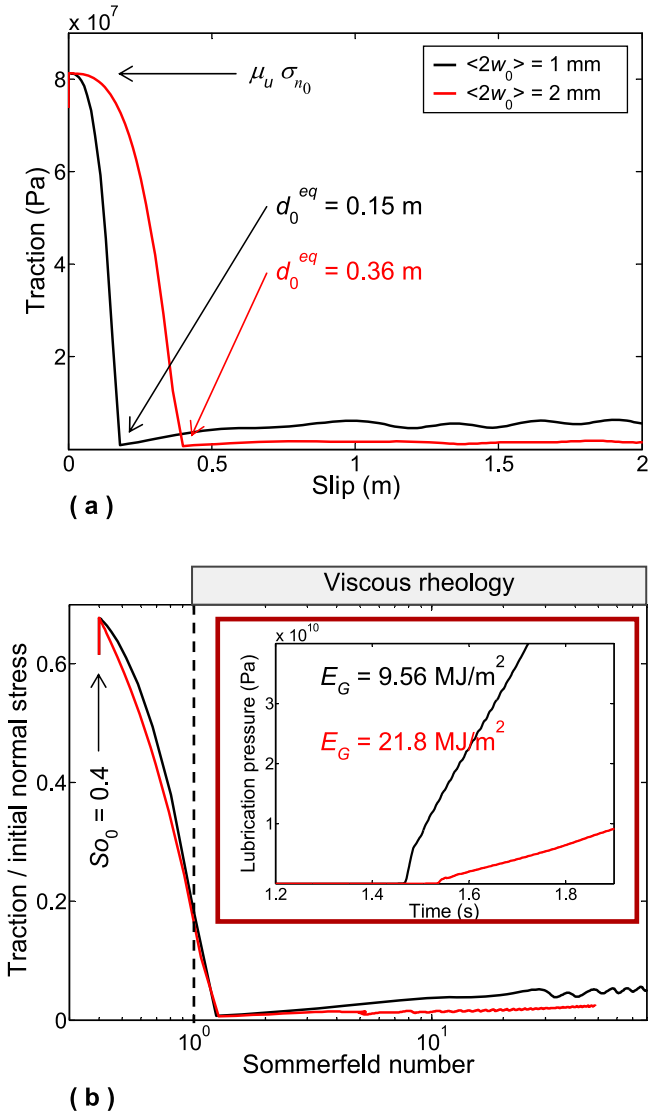

Figure 8. The same as Figure 7, but now we change the value of the average gap height $\langle 2w_0 \rangle$. In this case $\eta = 25$ Pa s.

[38] We emphasize that in spontaneous models the velocity history is a priori unknown and therefore the above-mentioned equation (9) can give us only qualitative information; quantitative estimates of the effects of η, r and $\langle 2w_0 \rangle$ on the time history of p_{lub} can be only obtained after the completion of a numerical experiments. Indeed, the time evolution of fault slip and slip velocity in a given fault node depend on the rupture propagation itself, in terms of the load exerted by the failing points (i.e., of the stress redistribution on the fault surface).

[39] Another interesting outcome is that all the numerical experiments predict the transition to a fully lubricated regime, in agreement with the theoretical prediction discussed in Appendix C. Moreover, once the fault has entered in the viscous regime it does not switch back to Coulomb rheology (in other words *So* remains greater than 1), as also previously obtained (see Figure 6a).

[40] We also notice that the fault restrengthening is negligible in these cases and therefore we do not observe the healing of slip. We will discuss this effect in more detail in next section.

5. Time Variable Gap Height

[41] In the present section we allow the average size of the gap height to vary through time, either non linearly (equation (6)) or linearly (equation (7)). The resulting lubrication pressure is expressed by $p_{lub}^{(IV)}$ of equation (A1) or by equation (11), respectively (see also Table 1 for a compendious summary of the analytical expressions). It is interesting to recall again that because, at a given time t, u is not spatially uniform over the fault, then equation (6) (and equation (7) as well) automatically introduces a spatial heterogeneity in the value of the thickness of the slurry film at time t. We also remark here that the dominant deformation mode which constrains the behavior of a fault is still unclear and it probably remains as a prominent problem in this field. The nonlinear increase of $\langle 2w \rangle$ (equation (6)) is due to the elastic deformation of the wall, which is reversible and thus cannot be observed in the faults after slip stops. On the other

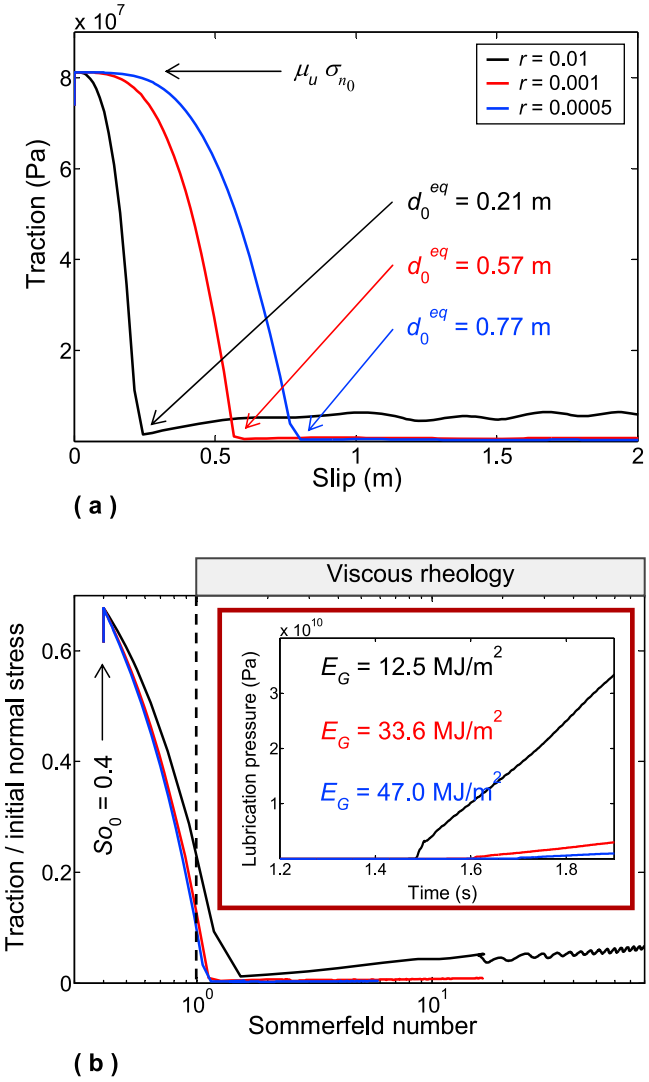

Figure 9. The same as Figure 7, but now we change the value of the roughness parameter r.

Table 2. Reference Parameters Adopted in the Present Study[a]

Parameter	Value
Medium and Discretization Parameters	
Lamé's constants, $\lambda = G$	35.9 GPa
Young's modulus, E	89.75 GPa
S wave velocity, v_S	3.464 km/s
P wave velocity, v_P	6 km/s
Fault length, L^f	16 km
Fault width, W^f	11.6 km
Spatial grid size, Δx	25 m
Time step, Δt	6×10^{-4} s[b]
Coordinates of the hypocenter, H $\equiv (x_1^H, x_3^H)$	(8, 7) km
Fault Constitutive Parameters	
Normal stress, σ_n	200 MPa[c]
Reference reservoir fluid pressure, p_{res}	80 MPa[d]
Initial lubrication pressure, p_{lub_0}	0[e]
Initial effective normal stress, $\sigma_{n_0}^{\mathrm{eff}} = \sigma_n - p_{res} - p_{\mathrm{lub}_0}$	120 MPa
Initial shear stress (pre-stress), τ_0	73.8 MPa
Static level of the friction coefficient, μ_u	0.677
Dynamic fluid viscosity of the slurry (reference), η	10 Pa s[f]
Initial average thickness of the slurry film (reference), $\langle 2w_0 \rangle$	2 mm
Roughness parameter, r	0.001[g]

[a]We assume that the medium surrounding the fault is homogeneous, isotropic and linearly elastic. The subscript 0 denotes the initial values (i.e., at t = 0).

[b]For the adopted parameters the Courant-Friedrichs-Lewy ratio, $\omega_{CFL} \underset{\mathrm{df}}{=} v_S \Delta t/\Delta x$, equals 0.083 and the estimate of the critical frequency for spatial grid dispersion, $f_{acc}^{(s)} = v_S/(6\Delta x)$, equals 23 Hz.

[c]This corresponds to a representative normal load of tectonic origin (i.e., lithostatic, overburden stress) at the hypocentral depth.

[d]Assuming hydrostatic conditions, as in *Brodsky and Kanamori* [2001].

[e]The resulting Sommerfeld number at $t = 0$ is then: $So_0 = 0.4$ (see equation (1)).

[f]In agreement with *Brodsky and Kanamori* [2001]. The dynamic viscosity of the slurry can also depends on the temperature (and thus on the depth) and on the solid volume fraction [*Guth and Simha*, 1936; *Major and Pierson*, 1992]. This estimate of the viscosity is necessarily approximate and therefore we explore the parameter space, by considering different values of η.

[g]Average value from the estimates of the roughness from 10^{-4} to 10^{-2} found by *Power and Tullis* [1991].

hand, the linear variation of $\langle 2w \rangle$ is based on the wearing process, which is irreversible and observables in the field. In this section we consider these two possible mechanisms, regarding them as end-members of the variations of the gap height. We can also guess that both effects may come into play in natural faults.

5.1. Nonlinear Variation of $\langle 2w \rangle$

[42] In Figure 10 we compare the results obtained by assuming a constant gap height (continuous lines) with those pertaining to a fault structure in which $\langle 2w \rangle$ follows equation (6). In spite of the rather different evolutions of $\langle 2w \rangle$ (reported in Figure 10a) the behavior of the rupture is quite similar in both of the cases; the rupture times are very similar, as well as the time evolution of the fault slip velocity and their peaks (see Figure 10b). Both of the models exhibit a transition to the viscous regime, which occurs nearly at the same time (marked by circles in the plots). While the Sommerfeld number increases in the case of constant $\langle 2w \rangle$, it decreases after its peak in the case of time variable thickness (see Figure 10c). This is justified by the rather different evolution of the lubrication pressure in the two cases (see the inset in Figure 10d). Physically, this is due to the increase of $\langle 2w \rangle$ which causes a reduction of p_{lub}, which in turn causes a decrease in So. Interestingly, the Sommerfeld number remains above the unity, so that the system does not switch again to a Coulomb rheology, but it continues to behave in a viscous fashion.

[43] Moreover, the slip-weakening curve reported in Figure 10d indicates that the initial roll-off, the equivalent slip-weakening distance, as well as the weakening rate are practically indistinguishable in the two models. Correspondingly, the fracture energy density is very similar, as reported in Figure 10d. All these similarities are due to the fact that the transition to the fully lubricated regime (which in turn represents the beginning of the significant difference between the two models) occurs nearly at the end of the breakdown process, when the stress drop is practically accomplished (see circles in Figure 10d). The different values of $\langle 2w \rangle$ cause then a slightly different evolution of the traction after the completion of the breakdown process (see Figure 10d), essentially due to the different evolution of p_{lub}.

[44] The two ruptures exhibit also a comparable evolution of the cumulative fault slip (Figure 10e). We can also see that the transition to the fully lubricated regime occurs before u exceeds the critical lubrication length (equation (8); dashed gray curve in Figure 10e).

[45] The results discussed above are general and not peculiar of the adopted parameters; as an overall conclusion we can highlight that the nonlinear increase of the gap height does not change the general behavior of the rupture, in terms of rupture speed, peaks in fault slip velocity, fracture energy density. Moreover, if the parameters of the model produce an increase of $\langle 2w \rangle$ with u too rapid, it might happen that the rupture is inhibited.

5.2. Linear Variation of $\langle 2w \rangle$

[46] When the gap height obeys equation (6) we do not have the possibility to directly control the rate of its increase with the fault slip, in that it explicitly depends on p_{lub}, which in turn is a priori unknown. On the contrary, equation (7) allows for a more direct control of the rate of increase of $\langle 2w \rangle$ with u, thought the input constant K.

[47] In Figure 11 we compare the results with a constant and variable $\langle 2w \rangle$ (black and color curves, respectively). As expected, for very low values of the constant K the solution is practically indistinguishable from the reference case, which has a constant thickness of the slurry film. For intermediate values we have a very similar evolution of the system, with the same slip velocity peaks and comparable values of the fracture energy density, although the lubrication pressure decreases after its peak. This result, obtained with $K = 0.0005$ (red curves in Figure 11), is very similar to that previously obtained with a nonlinear variation of $\langle 2w \rangle$ (see Figure 10). Also in this case the decrease of p_{lub} is not so dramatic to cause the Sommerfeld number to fail again in the range $So < 1$.

[48] A different situation is represented by the case of sustained increase of $\langle 2w \rangle$; with $K = 0.001$ (blue curves in Figure 11) the initial response of the fault is similar, in that we have an abrupt increase of the fault slip velocity (which reaches roughly the same peak as in the reference case; Figure 11b), the transition to the regime of $So > 1$ (Figure 11c) and a dramatic fault weakening (Figure 11d). However, the significant increase of $\langle 2w \rangle$ (reported in

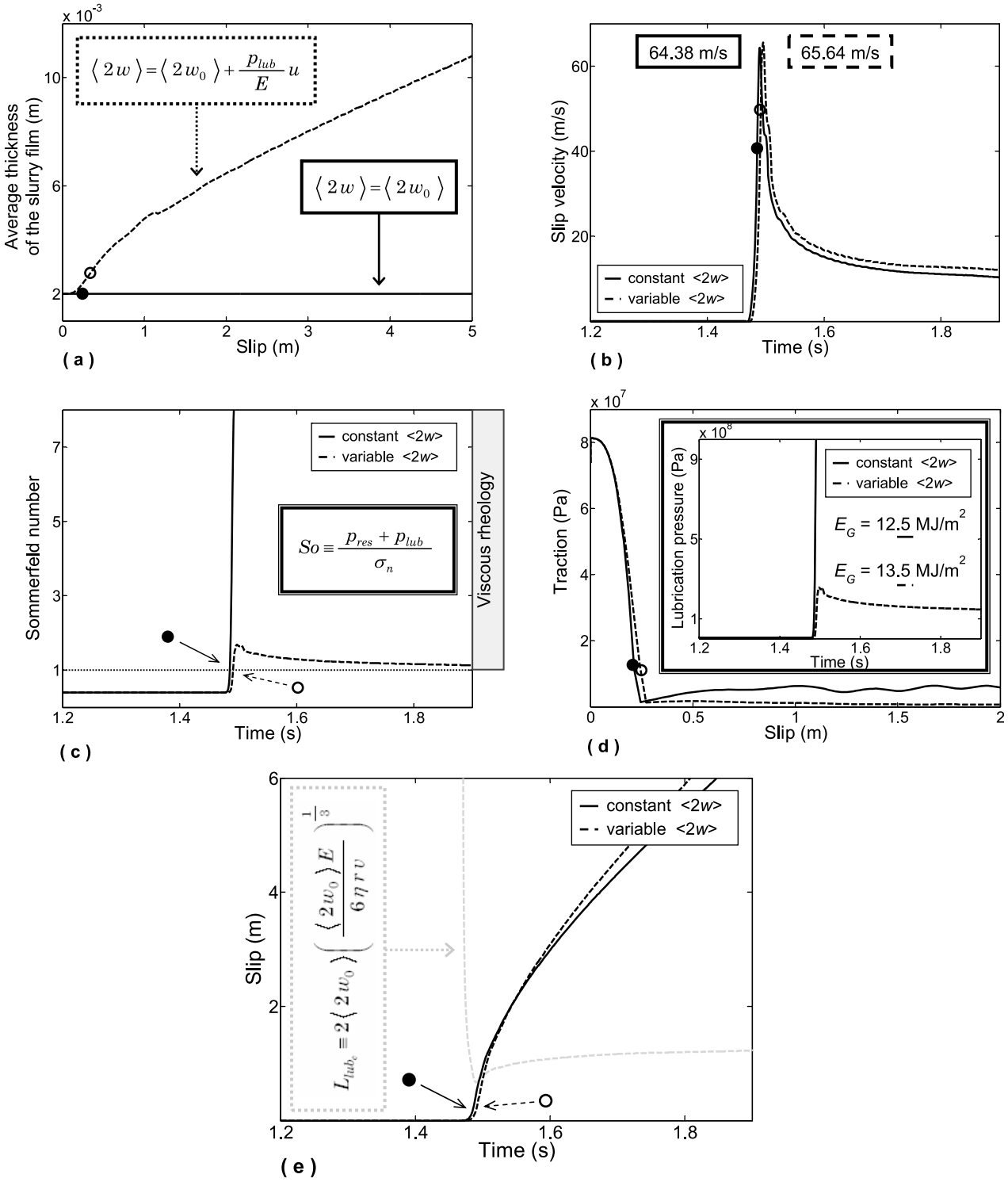

Figure 10. Comparison between a case with constant and a variable thickness of the slurry film (solid and dashed lines, respectively). (a) Evolution of $\langle 2w \rangle$ as a function of the slip. (b) Time history of the fault slip velocity, with the indication of the peaks. (c) Time evolution of the Sommerfeld number *So*. (d) Slip-weakening curve, with inset panel reporting the time evolution of the lubrication pressure and the resulting fracture energy densities. The small oscillations of the traction after the completion of the stress release are purely numerical. In all panels the circles denote the time when occurs the transition to the fully lubricated regime (i.e., when $So > 1$). The solutions refer to the same fault receivers as in Figures 7, 8 and 9. In this case $r = 0.01$. (e) Time evolution of the slip, compared (for the case of time variable $\langle 2w \rangle$) with the corresponding evolution of the critical lubrication length (equation (8)).

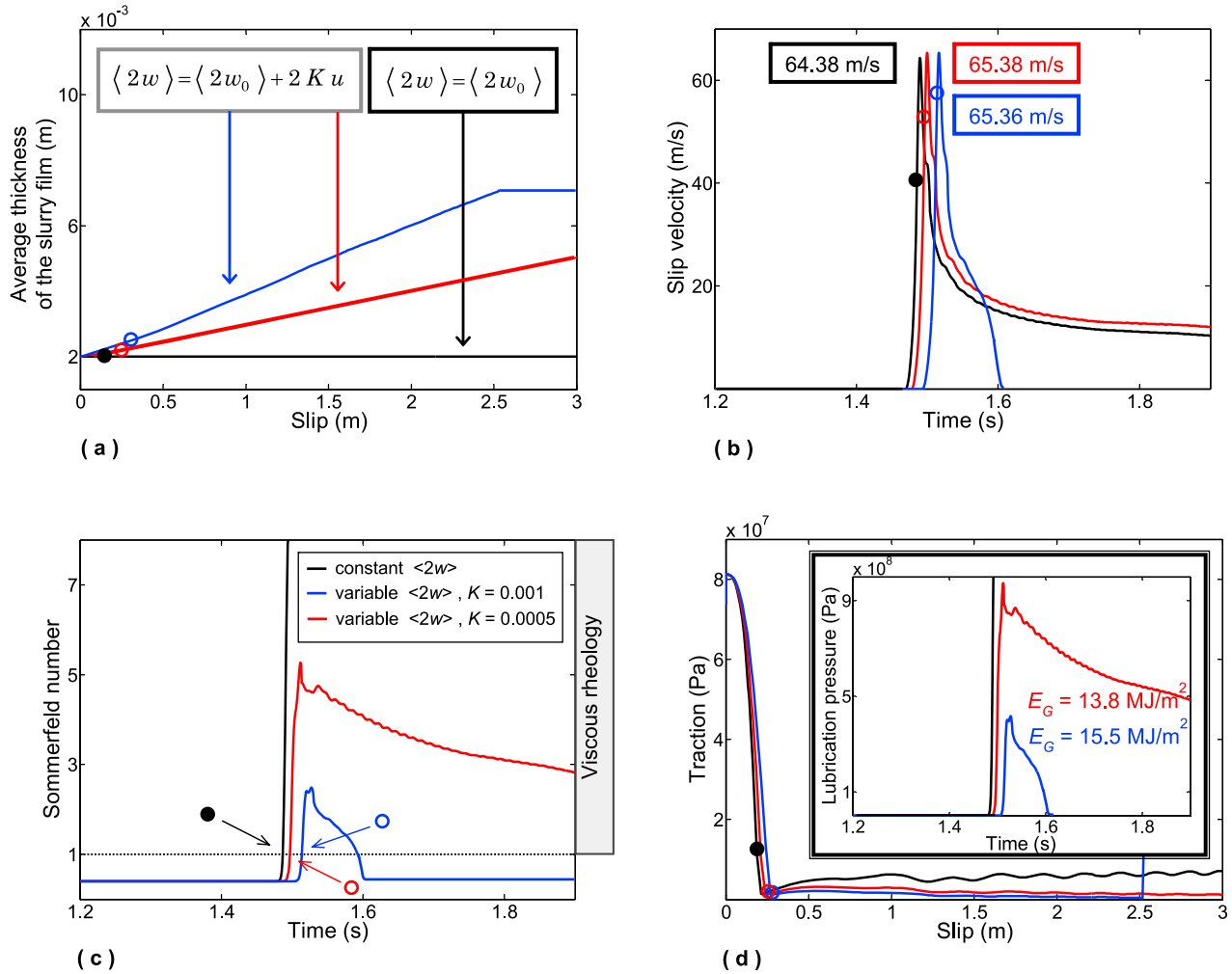

Figure 11. The same as in Figure 10, but now for a linear variation of $\langle 2w \rangle$ with the cumulated fault slip (equation (7)).

Figure 11a) causes p_{lub} to decrease significantly (inset in Figure 11d), so that the system experiences again the transition through So = 1 (Figure 11c). Correspondently, the traction exhibits a restrengthening and the slip heals (see Figures 11d and 11b, respectively). At that time, as stated by equation (7), the gap height no longer widen (Figure 11a).

6. Discussion and Conclusions

[49] In the present work we analyze the behavior of fully dynamic earthquake ruptures, which spread spontaneously on faults where the lubrication is active. The physical model introduced here (explained in detail in section 2) accounts for a possible transition between a Coulomb-based friction and a fully lubricated (viscous) rheology. This transition is spontaneous and it depends on the adopted parameters and thus on the resulting rupture history. We consider both a temporally constant width of the slurry film (section 4) and models where it varies as a function of the cumulated slip (section 5).

[50] The use of the scaling relation derived by *Brodsky and Kanamori* [2001] — upon which the model developed here is based — simplifies the complete problem, which would require the solution of the Navier-Stokes equations for the slurry entrapped within the slipping zone in all fault nodes and for a specific topology of the sliding surfaces. Nevertheless, the model presented here makes it possible to quantitatively evaluate the effects of lubrication on the cosesimic response of a fault.

[51] The adopted constitutive model accounts, within the Coulomb range, for possible variations of effective normal stress (σ_n^{eff}) due to variations of the lubrication pressure (see equation (2)). Temporal changes of σ_n^{eff} have been also explored in laboratory experiments, where the normal load was varied through time [*Linker and Dieterich*, 1992; *Prakash and Clifton*, 1992; *Prakash*, 1998; *Richardson and Marone*, 1999; *Bureau et al.*, 2000] as a boundary condition.

[52] In the framework of our model we have obtained some interesting results which are summarized below.

6.1. Theoretical Remarks

[53] The lubrication model adopted in the present paper formally is a slip- and velocity-dependent friction model. Indeed, we know that purely rate-dependent friction is in contrast with laboratory evidences [e.g., *Ohnaka*, 2003], in that friction is not a one-valued function of v (see also the discussion in *Bizzarri* [2011b]). As discussed above, a

purely rate-dependent model can be very unstable for low values of the slip rate, as discussed in detail by *Cochard and Madariaga* [1994] and *Madariaga and Cochard* [1994]. While a trivial extension of the analysis of *Rice et al.* [2001, section 3.2] suggests the possibility of ill-posedness in some slip- and velocity-dependent friction problems, the high resolution simulations shown here present no sign of ill-posedness (e.g., absence of short wavelength oscillations of slip rate in Figures 10b and 11b). Indeed, for slip-dependent friction models, an important indication of the resolution of the numerical simulations is represented by the number of points we have in the so-called cohesive zone, where the breakdown process is accomplished [e.g., *Bizzarri et al.*, 2001; *Bizzarri and Cocco*, 2005; *Day et al.*, 2005]. For each simulations presented in the present paper, we verify that the breakdown phase is properly resolved for the adopted parameters and for the given spatio-temporal resolution. Overall, we always have not less than 30 points within the equivalent slip-weakening distance.

[54] The physical model presented in this paper is inherently different with respect to another model where a viscous behavior is considered, i.e., a model accounting for the formation of a layer of molten fault products [*Bizzarri*, 2011a, and references therein]. As discussed in Appendix B, the former model considers a low viscosity slurry ($\eta = 10$–50 Pa s), which has been formed from liquids permeating the fault structure and debris and other tribological products of faulting. On the contrary, the latter model accounts for the melting of such tribochemical products in a dry ambient, which causes the spontaneous transition between a Coulomb-based rheology to a viscous shear, controlled by the evolution of a high viscosity melt layer (for frictionally molten materials the dynamic viscosity typically is $\sim 10^4$ Pa s).

[55] On the other hand, the lubrication model differs also from the thermally-activated pore fluid pressurization [e.g., *Lachenbruch*, 1980; *Bizzarri and Cocco*, 2006; *Rice*, 2006]. In the framework of our physical model we assume that the slurry is already present in the fault structure (at the beginning of the sliding pertaining to the actual earthquake process). Due to its high viscosity (compared to the viscosity of the water), the slurry, composed by the gouge particles and the remaining liquids, cannot be squeezed through the thermal pressurization mechanism and its acts as a lubricant. The basic idea behind the constitutive model proposed in this paper is that the viscosity of the slurry is not so sensitive to the mean stress that we can treat it as a Newtonian fluid; this is physically reasonable, at least to the first order [*Brodsky and Kanamori*, 2001]. There is evidence of slurries in fault zones viscous enough to produce lubrication [e.g., *Major and Pierson*, 1992]. A more complicated model would include, in the simulation of the same earthquake rupture, both the thermal pressurization process and the subsequent lubrication phenomenon, once the fluids have been squeezed out of the slipping zone and the slurry has formed. Here we have conservatively assumed the slurry is already formed at the beginning of the actual earthquake.

[56] At a more fundamental level, the most relevant theoretical outcome of the constitutive model presented here is that it allows for the analysis of the fault dynamics also when the magnitude of the effective normal stress approaches zero or it would tend to become negative. In the framework of a purely Coulomb rheology this should imply the opening or the interpenetration of the materials, i.e., the coupling between shear to tensile (i.e., mode I) modes of fracture [e.g., *Yamashita*, 2000; *Vavryčuk*, 2011]. In this light, the lubrication can be regarded as an alternative to this situation, in that it is assumed that the solid-solid friction is no longer valid for large Sommerfeld numbers (see equation (1)) and the fault obeys a viscous rheology.

6.2. Shape of the Slip-Weakening Curve

[57] The governing model presented here is able to capture the weakening behavior of the fault experiencing a seismic rupture, but it does not include the initial slip-hardening stage. This preparatory phase, during which the frictional resistance increases logarithmically with time [*Dieterich*, 1972; *Beeler et al.*, 1994; *Karner et al.*, 1997; *Karner and Marone*, 1998; *Marone*, 1998], has been interpreted as a result of the time-dependent growth of the real asperity contact area between the two opposite rock walls and between the grain particles comprising gouge materials [*Mizoguchi et al.*, 2009]. The present constitutive model assumes that the fault is already prone to rupture, as for the slip-weakening functions [*Ida*, 1972; *Ionescu and Campillo*, 1999].

[58] Our spontaneous model predicts that the slip-weakening curve does not follow an exponential weakening, both in the case of constant and variable thickness of the slurry film (Figures 7a, 8a, 9a, 10d, and 11d). The only exception is represented by the case of variable $\langle\, 2w \,\rangle$ but with imposed slip velocity history (see Figure 5e); when v is not imposed but is itself a solution of the problem then the weakening is abrupt and does not have an exponential behavior.

[59] This can be explained by looking at Figure 12, where we plot the evolution, as a function of the cumulated fault slip up to the completion of the breakdown phase, of the three terms which determine the frictional resistance. For sake of simplicity we consider the case of constant $\langle\, 2w \,\rangle$, with the reference parameters tabulated in Table 2 (this corresponds to the black line in Figure 7). We can clearly see that the second term of equation (10), which predicts a parabolic slip-dependence (i.e., like $-u^2$), is the most important contribution in τ and it is definitively paramount with respect to the third term, which tends to compensate the previous one with a linear slip-hardening. We note that the third term seems to be a horizontal line only for the selected scale in the ordinate axis; while its maximum value is nearly equal to 4.5×10^5 Pa, that of the second term in equation (10) is, in modulus, of the order of 10^8 Pa.

[60] Interestingly, the behavior of the slip-weakening curve we retrieve from our numerical experiments recalls very closely the functions 4 or 5 of *Ida* [1972, Table 1 and Figure 2]. Moreover, we highlight that the lubrication model exhibits a roll-off in the slip-weakening curve, in that the traction remains close to $\mu_u \sigma_{n_0}$ for a while, when the fault starts to slip. This kind of roll-off resembles the behavior postulated by *Ionescu and Campillo* [1999], who proposed a non-linear slip-dependent law which incorporates a sine-like weakening:

$$\tau = \begin{cases} \left[\mu_u - \dfrac{\mu_u - \mu_f}{d_0}\left(u - \dfrac{(1-p_{IC})d_0}{2\pi}\sin\left(\dfrac{2\pi u}{d_0}\right)\right)\right]\sigma_n^{eff} & ,u < d_0 \\ \mu_f \sigma_n^{eff} & ,u \geq d_0 \end{cases} \tag{12}$$

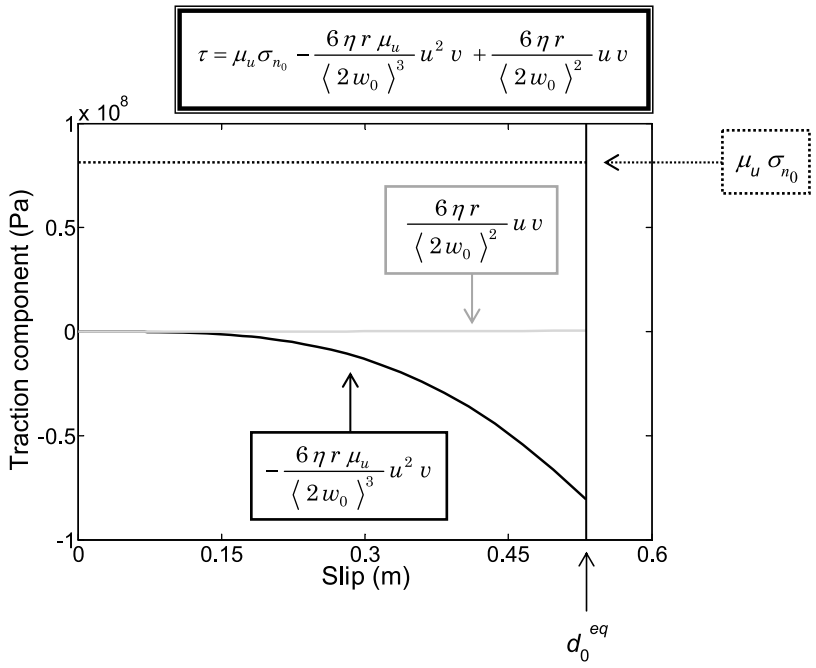

Figure 12. Behavior (as a function of the cumulated fault slip) of the three terms which determine the frictional resistance τ in the case of a constant gap height (in such a case τ is expressed as in equation (10)). The adopted parameters pertain to the reference case of Table 2 (black line in Figure 7).

where $p_{IC} \in [0, 1]$ and d_0 is the characteristic slip-weakening distance of the model. Finally, we report that a similar evolution of traction with the fault slip has been also considered by *Dunham* [2007, equation (14), with $p = 2$].

6.3. Dramatic Fault Weakening and Low Friction

[61] A reasonable approximation of the Byerlee' s laws states that the friction coefficient at the depth of a typical continental seismogenic zone, with the exception of a number of phyllosilicate minerals, roughly equals 0.75 [*Sibson*, 1974], an average value within the interval [0.6, 0.85] [e.g., *Scholz*, 2002]. The applicability to natural fault systems of such a value has been questioned and still remains a subject of an intense debate; indeed, laboratory evidences show a dramatic reduction of the friction coefficient [*Goldsby and Tullis*, 2002] (see also *Di Toro et al.* [2011] for a summary). Additionally, other studies revealed a low value of fault friction; in-situ stress measurements at boreholes drilled along the fault after the 1995 Kobe, Japan, EQ indicate that the residual friction was less than 0.3 [*Ikeda et al.*, 2001; *Yamamoto and Yabe*, 2001]. More recently, *Copley et al.* [2011] estimate a value roughly of 0.08 for the 2011 Bhuj, India, EQ, and *Suppe* [2007] concluded that the topography in Taiwan is supported by faults with friction lower than 0.04. It is interesting to emphasize that such a dramatic fault weakening has never been observed in the so-called conventional rock friction laboratory experiments [e.g., *Lockner and Beeler*, 2002], conducted under slow slip rates ($v \ll 1$ m/s).

[62] Our numerical experiments predict a nearly complete stress drop, as shown in Figures 7b, 8b, 9b, 10d, and 11d. Indeed, depending on the adopted parameters, we obtain a final traction after the completion of the breakdown process roughly of the order of 1–1.2 MPa (which, in a Coulomb range, would correspond to a value of 0.008–0.01 for the friction coefficient). Although the static stress drop for most earthquakes is generally assumed to fail in the range 1–10 MPa [*Kanamori and Anderson*, 1975; *Hanks*, 1977; *Abercrombie and Leary*, 1993], higher stress drop have been reported [*Kanamori et al.*, 1990; *Wald*, 1992; *Nadeau and Johnson*, 1998]. The low value of τ predicted by our model causes the ruptures to behave as supershear earthquakes.

[63] In the framework of the classical linear slip-weakening model [*Ida*, 1972], it is well-known that the occurrence of the supershear transition is basically controlled by the value of the strength parameter, which represents the ratio between the strength excess and the dynamic stress drop (see equation (15) in *Bizzarri* [2011b] and references cited therein). As a consequence, the supershear transition also depends on the initial level of stress on the fault. We emphasize here that in the present model the final level of stress is not prescribed, as in the case of the linear slip-weakening friction law, but it is itself a part of the solution. The same occurs for other governing models, such as the flash heating of asperity contacts and melting of rock and gouge, which also exhibit a dramatic fault weakening [*Andrews*, 2002; *Bizzarri and Cocco*, 2006; *Bizzarri*, 2009; *Rice*, 2006; *Bizzarri*, 2011a]. Indeed, *Bizzarri and Spudich* [2008] have shown that the inclusion of the thermal pressurization of the pore fluids can cause a supershear regime in a configuration which would produce a subshear propagation when the fluid migration is ignored (so that a linear slip-weakening governs the fault), regardless the value of the initial shear stress.

[64] We have also considered different configurations in which the initial shear stress on the fault is much lower than

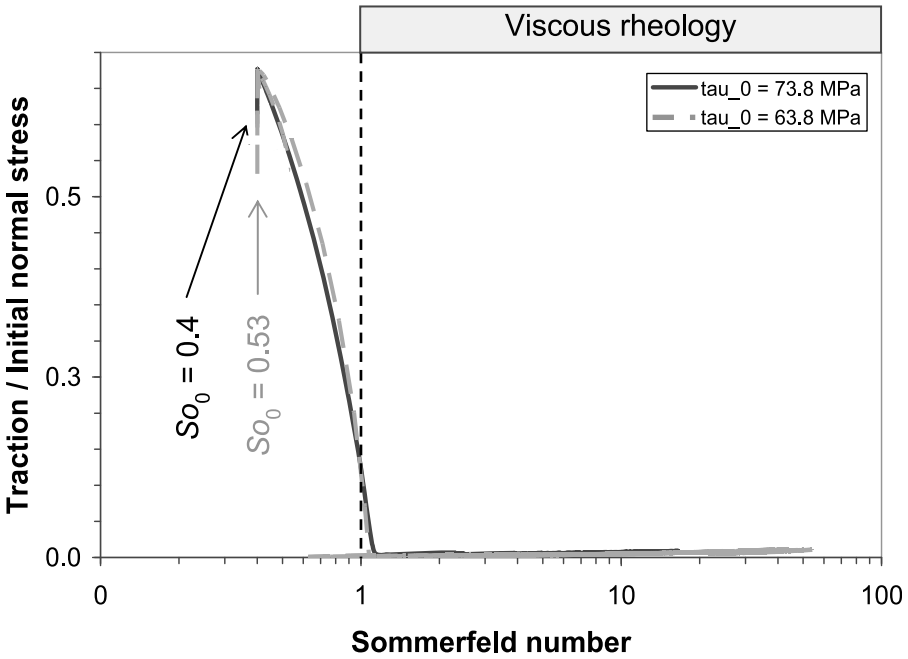

Figure 13. Comparison between a reference configuration having τ_0 = 73.8 MPa and a simulation with τ_0 = 63.8 MPa. The two Stribek curves are nearly coincident, indicating that the final level of friction is roughly the same in both models.

that assumed in sections 4 and 5. The results indicate that if τ_0 is too low, the rupture cannot be able to propagate outside the nucleation zone and immediately dies; this is due to the fact that the fault strength remains at a relatively high level for a significant amount of slip, after the rupture onset (see the roll-off in Figures 7a, 8a, 9a, and 10d). On the other hand, if the rupture spontaneously propagates outside the initialization zone, the breakdown stress drop is dramatic, so that supershear propagation is favored. This is clearly visible from Figure 13, where we superimpose the Stribek curves pertaining to the reference configuration (solid black curve) and to a fault with τ_0 = 63.8 MPa (dashed gray curve). We emphasize here that the generation of sub-Rayleigh ruptures might require incorporating in the current model other weakening mechanisms that facilitate the nucleation at low background stress.

[65] The low value of the shear traction can in some sense help to solve the heat flux paradox, i.e., the high temperatures developed during frictional sliding. Indeed, a low value of the traction can potentially counterbalance the high value of fault slip velocity (see section 6.5) and decrease the heat input term, which is directly proportional to the product τ *v*. Unfortunately, the chemical and physical properties of the slurry are very poorly understood and moreover they depend on its mineral composition, temperature and pressure conditions, water content, so that the temperature developed within the slipping zone (permeated by the slurry) is extremely difficult to be estimated.

6.4. Fracture Energy Density

[66] The dramatic fault weakening we obtain implies a high value of the so-called fracture energy density E_G [see *Bizzarri*, 2010d, and references therein]. To evaluate E_G we use $d = d_0^{eq}$ and $\tau_{res} = \tau_f^{eq} = \tau(u = d_0^{eq})$ in equation (1) of *Bizzarri* [2010d]. In our simulations we obtain values within the range 9.56–47.0 MJ/m^2, which are comparable with those obtained in synthetic earthquakes of the same magnitude ($M_0 \sim 10^{19}$ Nm or $M_w \sim 6.8$), obeying the Ruina-Dieterich governing model with the flash heating of microasperity contacts [*Bizzarri*, 2010d].

6.5. High Peak Slip Velocities

[67] As for the flash heating mechanism [*Bizzarri*, 2009; *Noda et al.*, 2009], also the lubrication model presented here predicts very high peaks of the fault slip velocity time history (v_{peak}). On average, our numerical experiments produce $v_{peak} \sim$ 50 m/s or even a little bit more, depending on the parameters assumed in the simulations. These values can be considered as overestimates of the peak slip velocity attained during a real earthquake. However, we remark here that these values have been obtained under the assumption that the whole fault contains the slurry; in other words, we hypothesize that the whole fault lubricates. Indeed, we can guess that during a natural earthquake only some patches of the fault are controlled by the lubrication processes [see also *Brodsky and Kanamori*, 2001; *Ma et al.*, 2003]; other portions of the fault, where lubrication is not active, provide lower values of v_{peak}.

[68] Our numerical experiments also indicate that the traction reached after the breakdown process (i.e., the so-called equivalent kinetic level) is attained when *v* reaches its peak, or even just before that time, depending on the parameters. As discussed by *Tinti et al.* [2004] this behavior is typical of supershear ruptures (as our ruptures are) and it has relevant seismological implications, in that we can use the time integration of *v* up to the time when v_{peak} is attained to

retrieve the (equivalent) slip-weakening distance, as early suggested by *Mikumo et al.* [2003].

6.6. Rapid Restrengthening and Healing of Slip

[69] Another interesting feature of the lubrication model proposed in this work is that it accounts for the possible fault restrengthening, occurring after the stress release. We have seen (dotted lines in Figures 2d, 3d, 4d, 5d) that when the slip velocity is forced to return to zero after some slipping time, then the frictional resistance increases, due to the decrease of the lubrication pressure. A similar rapid restrengthening, occurring just after the dynamic weakening, has been also observed in high-velocity laboratory experiments [*Hirose and Bystricky*, 2007; *Mizoguchi et al.*, 2009].

[70] When the fault slip velocity is not imposed (see sections 4 and 5) and the properties of the fault are homogeneous there is no any healing process, when the gap height is constant through time; in such a situation the rupture behaves as a classical enlarging crack. On the contrary, for linearly increasing thickness of the slurry film, we can have the cessation of slip (see Figure 11b, blue curve). Indeed, the increase in $\langle\ 2w\ \rangle$ causes p_{lub} to decrease and finally the frictional resistance to increase (see Table 1; last row). The healing of slip is obtained in cases when the enlargement of $\langle\ 2w\ \rangle$ occurs at a sufficiently high, but not too high, rate (for our parameters this occurs for $K \geq 0.001$).

[71] Interestingly, we also highlight that if the gap height increases too rapidly — due to the value of the parameters η, $\langle\ 2w_0\ \rangle$ and r in the case of a nonlinear increase, equation (6), or due to the value of the parameter K in the case of linear increase, equation (7) — the rupture can be inhibited. This can be interpreted also in the light of the discussion in Appendix C; while in the case of constant gap height we can a priori predict that the fault will enter the fully lubricated regime, when $\langle\ 2w\ \rangle$ varies this transition is not always guaranteed.

6.7. Future Perspective

[72] The next step of this research, which in some sense reciprocates the stimulating suggestion of *Hirose and Shimamoto* [2005], is to perform laboratory experiments simultaneously at high normal stress (>50 MPa) and with realistic time histories of slip velocity having peaks in the seismic range (1–20 m/s) and to check whether the theoretical results obtained here can explain the observation. This will certainly be a great challenge for the experimentalists in the near future.

Appendix A: Analytical Solution for the Lubrication Pressure When the Gap Height Evolves Following Equation (6)

[73] As mentioned in section 2, if the thickness of the slurry film is constant through time (i.e., $\langle\ 2w\ \rangle = \langle\ 2w_0\ \rangle$, $\forall t \geq 0$), equation (4) has the trivial solution reported in equation (9). On the other hand, when $\langle\ 2w\ \rangle$ linearly evolves with the slip as in equation (7) the solution for the lubrication pressure is also simple (see equation (11)).

[74] In the most general case, in which $\langle\ 2w\ \rangle$ nonlinearly evolves accordingly to equation (6), the solution of equation (4) is more elaborated, but can be still written in an analytical closed-form. Namely, by solving the coupled equations (4) and (6) we have four roots for p_{lub}, as listed below:

$$\begin{aligned} p_{\mathrm{lub}}{}^{(\mathrm{I})} &= -\frac{3}{2}\,a - l - m \\ p_{\mathrm{lub}}{}^{(\mathrm{II})} &= -\frac{3}{2}\,a - l + m \\ p_{\mathrm{lub}}{}^{(\mathrm{III})} &= -\frac{3}{2}\,a + l - n \\ p_{\mathrm{lub}}{}^{(\mathrm{IV})} &= -\frac{3}{2}\,a + l + n \end{aligned} \tag{A1}$$

where

$$\begin{aligned} a &\equiv \frac{\langle\ 2w_0\rangle\ E}{2\,u} \\ l &\equiv \frac{1}{2}\,\sqrt{a^2 - b + c} \\ m &\equiv \frac{1}{2}\,\sqrt{2a^2 + b - c - \frac{a^3}{l}} \\ n &\equiv \frac{1}{2}\,\sqrt{2a^2 + b - c + \frac{a^3}{l}} \end{aligned} \tag{A2}$$

with

$$\begin{aligned} b &\equiv 4\left(\frac{2}{3}\right)^{\frac{1}{3}}\left(\frac{2E^2\,\eta\,r\,v}{\langle\ 2w_0\ \rangle}\right)^{\frac{2}{3}}\frac{1}{q} \\ c &\equiv 2^{\frac{2}{3}}\left(\frac{3\langle\ 2w_0\ \rangle^2 E^5\,\eta\,r\,v}{4}\right)^{\frac{1}{3}}\frac{q}{u} \\ q &\equiv \left(\sqrt{1 + \frac{512\eta\,r\,u^3\,v}{9\langle\ 2w_0\ \rangle^4\,E}} - 1\right)^{\frac{1}{3}} \end{aligned} \tag{A3}$$

A detailed analysis of the solutions (equation (A1)) indicates that two solutions ($p_{lub}^{(\mathrm{I})}$ and $p_{lub}^{(\mathrm{II})}$) are complex-conjugate; this is due to the fact that m is imaginary. On the contrary, the two remaining solutions ($p_{lub}^{(\mathrm{III})}$ and $p_{lub}^{(\mathrm{IV})}$) are real-valued functions; of these, only $p_{lub}^{(\mathrm{IV})}$ is positive and can be therefore regarded as the physically admissible solution of equation (4).

[75] To quantitatively illustrate the behavior of the solutions (equation (A1)) we consider again three time velocity histories reported in Figure 1. The results are shown in Figures A1 and A2, where the different colors distinguish the four solutions (equation (A1)) and the style of the lines refers to the different time series reported in Figure 1. We can clearly see from Figure A1 that for all the considered time velocity histories $p_{lub}^{(\mathrm{I})}$ and $p_{lub}^{(\mathrm{II})}$ are imaginary functions with the same absolute value of the imaginary part (i.e., complex-conjugate). On the other hand, from Figure A2 we have that of the two real-valued solutions, $p_{lub}^{(\mathrm{III})}$ has negative or null values. On the contrary, $p_{lub}^{(\mathrm{IV})}$ is positive and thus physically admissible. This holds for all the three, rather different, time velocity histories we have considered (see Figure 1).

[76] In the numerical simulations presented in the paper having a time variable gap height we therefore consider the analytical expression of $p_{lub}^{(\mathrm{IV})}$ in the constitutive model (3).

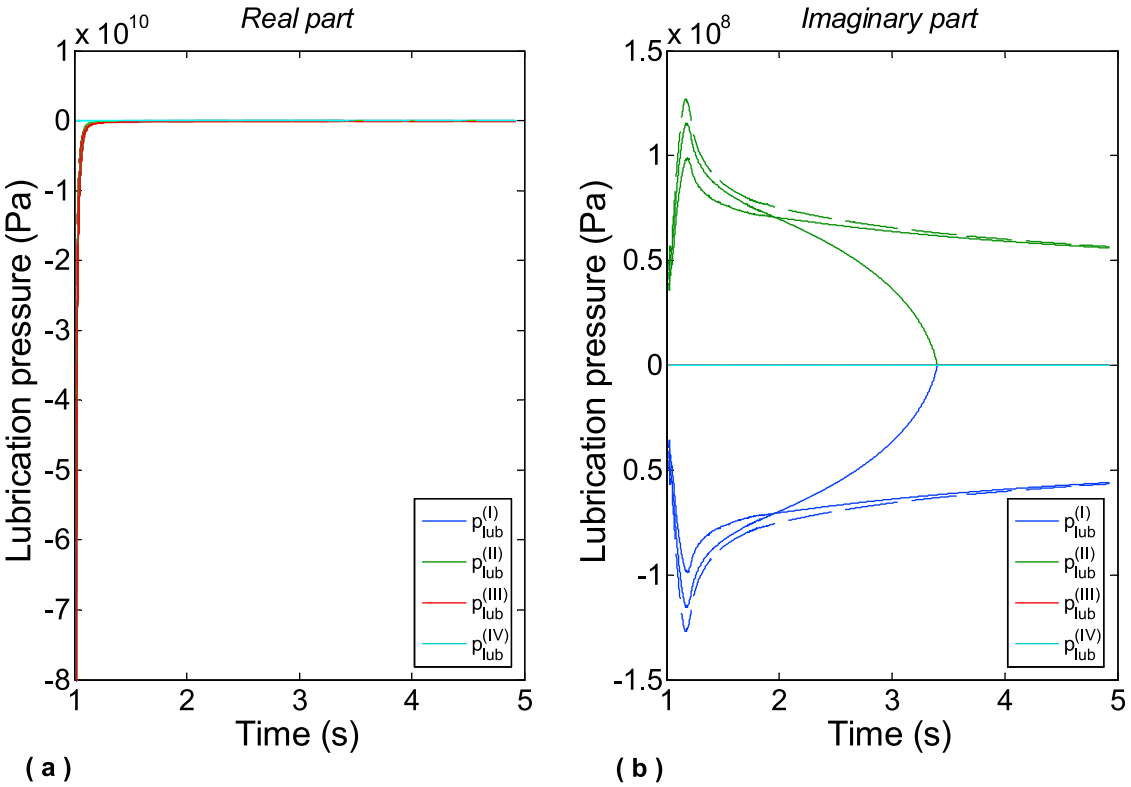

Figure A1. Time behavior of the four solutions (equation (A1)) of equation (4) for the typical slip velocity time histories reported in Figure 1 (the different style of the lines refers to the three cases reported in Figure 1). (a) Real part of the solutions. (b) Imaginary part of the solutions.

For a typical evolution of fault slip and fault slip velocity, a detailed analysis of the various terms appearing in $p_{lub}^{(IV)}$ indicates that all of them (a, b, c, l, n, q) are relevant and none of them can be neglected in the calculations of the lubrication pressure; therefore the encoding contains the full analytical expression of $p_{lub}^{(IV)}$ as given in equations (A1)–(A3).

[77] Interestingly, we also emphasize here that for vanishing values of u and v the function $p_{lub}^{(IV)}$ goes to zero; this is physically reasonable, in that at the very beginning of the rupture the lubrication is negligible and therefore the effective normal stress equals the reference value of σ_{n_0}, as in the case of constant thickness of the slurry film (see equation (10)).

Appendix B: Comparison With Other Weakening Mechanisms

[78] In this section we compare the traction evolution predicted by the lubrication model presented in this paper with other weakening mechanisms previously introduced in

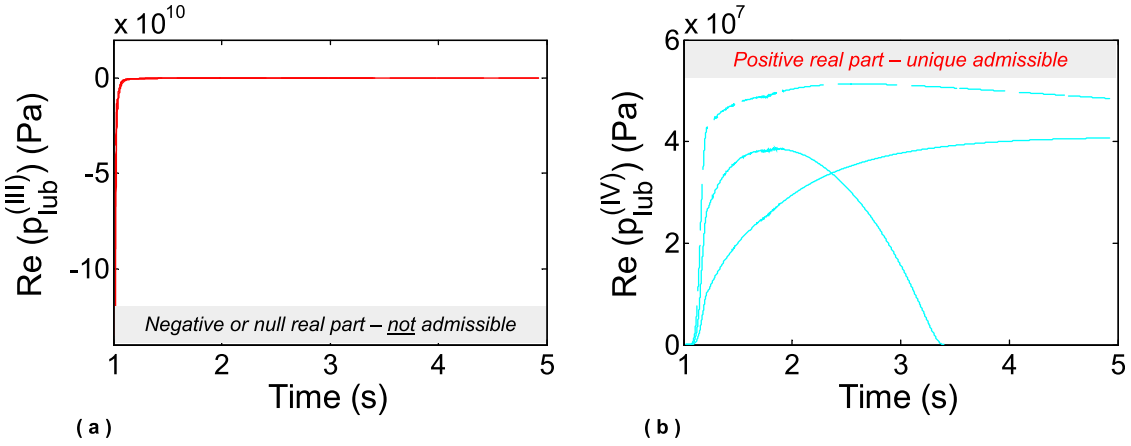

Figure A2. Time behavior two real-valued solutions (equation (A1)), again for the three velocity time histories of Figure 1. (a) Only $p_{lub}^{(IV)}$ has positive values and therefore it is the only admissible solution of equation (4); (b) $p_{lub}^{(III)}$ always has negative values.

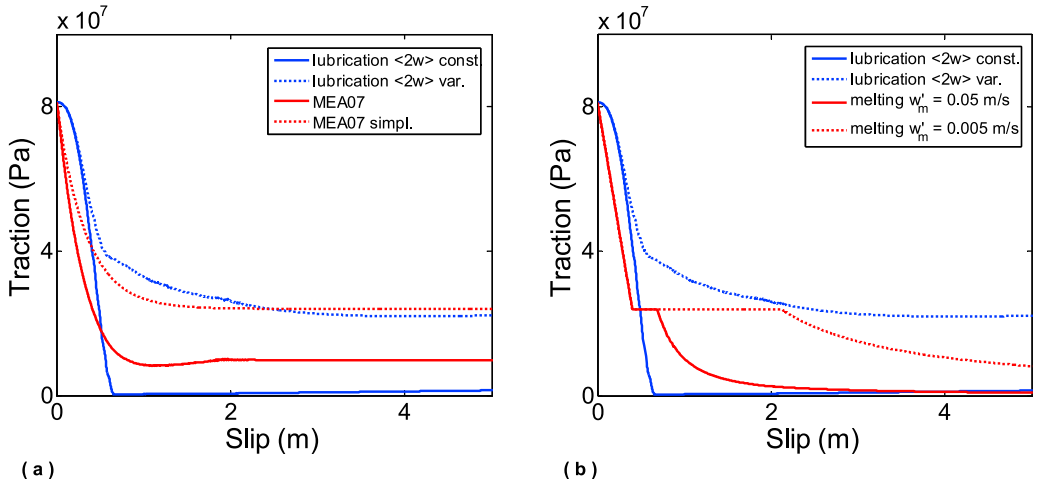

Figure B1. Comparison between the lubrication model presented in this paper (blue lines), (a) the exponential weakening (red lines) and (b) melting model (red lines). In the case of the lubrication model we assume either a constant and variable thickness of the slurry film (continuous and dotted lines, respectively), with the reference parameters tabulated in Table 2 and $r = 0.01$. In Figure B1a the dotted red line identifies the constitutive model (equation (B1)) and the continuous red line a more elaborated version of it, as in equation (B3). In Figure B1b the red lines denote the viscous evolution of traction as in equation (B4), for two representative values of the melting layer enlargement rate (see *Bizzarri* [2011a] for further details on the physical model of melting). In all cases the fault slip velocity is imposed and it is the continuous line in Figure 1. For the exponential weakening the parameters are the same as in *Bizzarri* [2010b]; $d = 1$ m, $\mu^{ss}(0) = 0.55$, $v_{SS} = 0.99$ m/s of $\mu_f = 0.2$. For the melting model the parameters are the same as in *Bizzarri* [2011a]; $\breve{\eta}_m = 1 \times 10^4$ Pa s and $w_m = \dot{w}_m(t - t_m)$, where $\dot{w}_m$ is enlarging rate of the molten layer, which equals 0.05 m/s or 0.005 m/s, and t_m is the time instant when the fault temperature exceeds the (average) melting point $T_m = 1200°$C. The fault temperature is computed as in equation (24) of *Bizzarri* [2011a], with a heat capacity per unit volume $c = 2.838 \times 10^6$ J/(m^3 °C) and a thermal diffusivity $\chi = 0.344 \times 10^{-6}$ m^2/s and by assuming, for simplicity, that the slipping zone thickness equals that of the slurry film.

the literature in the framework of governing laws with slip and velocity dependencies.

B1. Exponential Weakening

[79] The exponential weakening (EW thereinafter) of the fault resistance has an ancient origin, in that it has been early postulated by *Lachenbruch* [1980] and then reconsidered by theoretical work by *Matsu'ura et al.* [1992]. More recently, *Rice* [2006] introduced this functional behavior to describe the thermal pressurization of faults. *Mizoguchi et al.* [2007], by fitting data from laboratory experiments conducted with a rotary-shear apparatus on samples with fault gouge collected from an outcrop of the Nojima fault, propose the following governing law [see also *Hirose and Shimamoto*, 2005]:

$$\tau^{(\mathrm{EW})} = \left[\mu_f + \left(\mu_u - \mu_f\right) \mathrm{e}^{\frac{\gamma u}{d}} \right] \sigma_n^{\mathrm{eff}} \tag{B1}$$

where μ_f is the residual level of the friction coefficient, $\gamma \equiv \ln(0.05)$ and d is a characteristic weakening distance. Equation (B1) has been further generalized by *Sone and Shimamoto* [2009], who include *i*) a slip-hardening effect, realized by substituting the constant term μ_u with the function

$$F(u) = \alpha_{\mathrm{SS}} + (1 - \alpha_{\mathrm{SS}}) \mathrm{e}^{\frac{\gamma u}{u_h}} \tag{B2}$$

(where α_{SS} and u_h are empirical constants which modulate the slip-hardening phase), and *ii*) a more complicated evolution of the final level of friction, obtained by replacing the term μ_f with a steady-state function

$$\mu^{\mathrm{ss}}(v) = \mu^{\mathrm{ss}}(0) \mathrm{e}^{-\frac{v}{v_{SS}}} \tag{B3}$$

where $\mu^{ss}(0)$ and v_{SS} are constants with values constrained experimentally.

B2. Melting of Rocks and Gouge

[80] By considering a perfectly drained configuration (i.e., by assuming that mechanisms of fluid circulations are unimportant), *Bizzarri* [2011a] proposes a physical model accounting for the spontaneous transition between a Coulomb and a viscous rheology when the melting of rocks and gouge occurs. This model for melting fault zone has been proved to show a sufficiently good agreement with field data collected on an exhumed seismic thrust fault zone in Outer Hebrides, Scotland, and with measurements from *Sibson* [1975], performed on the same fault zone.

[81] In particular, when an effective melting temperature (formally defined as in equation (23) of *Bizzarri* [2011a]) is exceeded, the frictional behavior is no longer based on the

Amonton-Coulomb-Mohr framework, but it is described as that of a viscous Newtonian fluid:

$$\tau^{(NF)} = \breve{\eta}\,\frac{v}{2w_m} \tag{B4}$$

where $\breve{\eta}$ is the dynamic viscosity of the molten material and w_m is the half-width of the melt layer, which progressively enlarges as the rupture propagates (see *Bizzarri* [2011a] for physical and analytical details). Of course, $\breve{\eta}$ is higher than the dynamic viscosity of the slurry considered the lubrication model introduced in section 2; in the case of isoviscous melt layer, typically $\breve{\eta} = \breve{\eta}_m = 1 \times 10^4$ Pa s [see also *Spray*, 1993].

B3. Numerical Comparison

[82] For sake of simplicity we assume that the fault slip velocity history is the continuous line in Figure 1. As for the results discussed in section 3, we hypothesize that the slip velocity is assigned for all the different constitutive formulations and it is not a part of the solution of the problem, as in the case of spontaneous models of ruptures. Once the slip velocity time history is given, we compute the resulting traction evolution and we compare the different governing models, the lubrication model either with constant and variable gap height (continuous and dotted lines, respectively) and the two models presented in previous subsections (red lines). The initial conditions are the same for all the governing laws.

[83] From Figure B1a we can clearly see that the simplified exponential weakening (equation (B1)), namely the governing model proposed by *Mizoguchi et al.* [2007], agrees very well with the lubrication model with enlarging $\langle\ 2w\ \rangle$ (dotted blue and dotted red curves, respectively). In both cases the decrease of the frictional resistance is continuous and the final level is roughly the same. When the final level of friction depends explicitly on the fault slip velocity, as in equation (B3), the traction drop predicted by the exponential weakening is more significant (continuous red curve), but still lower than that predicted by the lubrication model with constant $\langle\ 2w\ \rangle$ (continuous blue curve). In the latter case there is a clear definition of the equivalent slip-weakening distance d_0^{eq} [*Bizzarri and Cocco*, 2003].

[84] As already discussed in *Bizzarri* [2011a], when the fault behaves as a Newtonian fluid the frictional resistance decreases significantly; this is visible from the red lines in Figure B1b. Interestingly, the final value of traction predicted by the melting model agrees very well with the prediction of the lubrication model with the constant thickness of the slurry film. On the contrary, when $\langle\ 2w\ \rangle$ varies the final traction is greater than that obtained with melting model, independently on the value of the enlarging rate of the molten layer $\dot{w}_m$.

Appendix C: Occurrence of the Transition to the Fully Lubricated Regime

[85] The focus of the present section is on the evaluation of the transition to the fully lubricated (viscous) rheology. Let the time at which such a transition occurs be indicated with the symbol t_t, which is formally defined as the first instant when $So = 1$. The fault slip developed at $t = t_t$ will be denoted with u_t thereinafter.

[86] In the particular case of constant $\langle\ 2w\ \rangle$, from equation (10) we have

$$u_t = \sqrt{\frac{(\sigma_n - p_{\mathrm{res}})\ \langle\ 2w_0\ \rangle^3}{6\,\eta\,r\,v_t}} \tag{C1}$$

being v_t the value of the fault slip velocity at $t = t_f$ (the other constants have been already defined above, but we recall here that σ_n is the normal stress, p_{res} is the reference pore fluid pressure of the reservoir in the far-field, $\langle\ 2w_0\ \rangle$ is the initial average thickness of the gap height, η is the dynamic viscosity of the of the slurry and r is the roughness parameter). When the velocity history is not imposed, as for the spontaneous ruptures considered in sections 4 and 5, obviously also v_t is a priori unknown. The corresponding value of fault traction τ_t can be expressed as it follows:

$$\tau_t = \sqrt{\frac{6\eta\,r\,v_t\,(\sigma_n - p_{\mathrm{res}})}{\langle\ 2w_0\ \rangle}}\ . \tag{C2}$$

Some complications arise in the case of time variable thickness of the slurry film; when its evolution follows equation (7) (i.e., a linear increase of $\langle\ 2w\ \rangle$ with the fault slip u with the rate of K) we have that u_t is the solution of the following equation:

$$\frac{(2K\,u_t + \langle\ 2w_0\ \rangle)^3}{{u_t}^2} = \frac{6\eta\,r\,v_t}{\sigma_n - p_{\mathrm{res}}}. \tag{C3}$$

Interestingly, we can note that equation (C1) always gives a real-valued and positive estimate of u_t , while equation (C3) has the three following roots

$$\begin{aligned}
{u_t}^{(\mathrm{I})} &= d\left(-a + 4b + \frac{a\,(a - 8b)}{\sqrt[3]{c}} + \sqrt[3]{c}\right)\\
{u_t}^{(\mathrm{II})} &= d\left(a - 4b + \frac{(1 + \mathrm{i}\sqrt{3})\,a\,(a - 8b)}{2\sqrt[3]{c}} + \frac{(1 - \mathrm{i}\sqrt{3})\ \sqrt[3]{c}}{2}\right)\\
{u_t}^{(\mathrm{III})} &= d\left(a - 4b + \frac{(1 - \mathrm{i}\sqrt{3})\,a\,(a - 8b)}{2\sqrt[3]{c}} + \frac{(1 + \mathrm{i}\sqrt{3})\ \sqrt[3]{c}}{2}\right)
\end{aligned} \tag{C4}$$

where

$$\begin{aligned}
a &\equiv \eta\,r\,v_t\\
b &\equiv \frac{K^2\ \langle\ 2w_0\ \rangle}{2}\ (\sigma_n - p_{\mathrm{res}})\\
c &\equiv 8\sqrt{a^2\,b^3\,(9b - a)} - a\left(a^2 - 12a\,b + 24b^2\right)\\
d &\equiv \frac{1}{4K^3\,(\sigma_n - p_{\mathrm{res}})}
\end{aligned} \tag{C5}$$

and i is the imaginary unit (i.e., $\mathrm{i}^2 = -1$). Independently on the value of the adopted parameters (η, r, K, σ_n and p_{res}), $u_t^{(\mathrm{I})}$ always is a negative real number (and thus is inadmissible by definition of the cumulated fault slip; $u \equiv \|\ \mathbf{u}\ \|$). $u_t^{(\mathrm{II})}$ and $u_t^{(\mathrm{III})}$ become pure-real numbers only after a critical value of the velocity v_t ; after such a value always is: $u_t^{(\mathrm{II})} > u_t^{(\mathrm{III})}$. In conclusion, we can regard $u_t^{(\mathrm{III})}$ as the admissible solution of

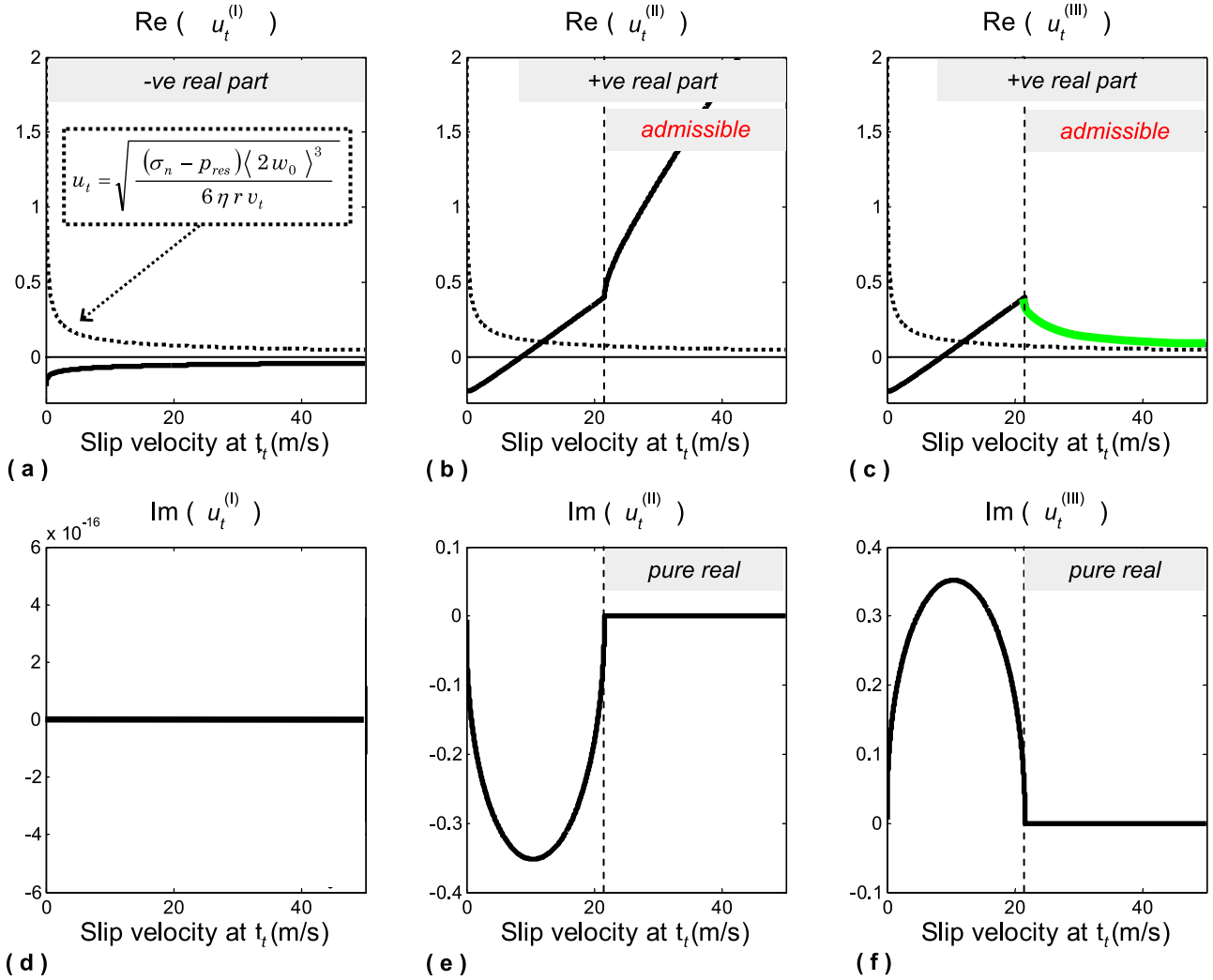

Figure C1. Behavior of the solutions (equation (C4)) for the cumulative fault slip developed when $So = 1$ for the first time in a model where $\langle 2w \rangle$ linearly enlarges with u (i.e., it evolves accordingly to equation (7)). The solutions are plotted as a function of the fault slip velocity v_t (see Appendix C for details). In Figures C1a–C1c we also report, for comparison, the behavior of u_t predicted by a model with constant thickness of the slurry film (equation (C1)). Vertical dashed lines in Figures C1b, C1c, C1e, and C1f mark the range of velocities where solutions are real-valued functions ($v > 21.6$ m/s). The thick line in Figure C1c emphasizes the admissible solution. The adopted parameters are those reported in Table 2, except for $\langle 2w_0 \rangle$ which equals 4 mm.

equation (C3), provided that the fault slip velocity history attains a value of v_t which makes $u_t^{(III)}$ a real number.

[87] In other words, we can conclude that a model with a constant gap height always predicts that the fault will reach the viscous regime (because the transitional value of slip u_t always exists). On the contrary, a model where $\langle 2w \rangle$ linearly enlarges as the rupture develops does not always guarantee that the fault enters the range $So \geq 1$; this can occur only for some specific time evolution of the rupture (which in turn gives values of v_t such that $u_t^{(III)}$ is a real-valued quantity).

[88] An example of such a behavior is reported in Figure C1, where we plot the three solutions (equation (C4)) as a function of the velocity v_t . Vertical dashed lines in Figures C1b, C1c, C1e, and C1f indicate the range of velocities where solutions are real-valued functions ($v_t > 21.6$ m/s). We can clearly see that in such a range $u_t^{(III)}$ is the admissible solution (thick line in panel (c)), in that it has values systematically lower than those attained by the function $u_t^{(II)}$. From this results we can a priori predict that a model with these parameters which produces fault slip velocities lower than 21.6 m/s will not definitively experience the transition to the fully lubricated regime.

[89] **Acknowledgments.** I have strongly appreciated the stimulating discussions with E. E. Brodsky about the lubrication model proposed with H. Kanamori in 2001. S. Bruni is warmly acknowledged for the help in the postprocessing of some results from the numerical simulations. I am grateful to the Editor, R. Nowack, the Associate Editor and two anonymous referees for their comments. I acknowledge R. Madariaga and the Associate Editor for intriguing discussions about the problem of ill-posedness in the framework of rate-dependent constitutive models.

References

Abercrombie, R., and P. Leary (1993), Source parameters of small earthquakes recorded at 2.5 km depth, Canjon Pass, Southern California: Implication for earthquake scaling, *Geophys. Res. Lett.*, *20*, 1511–1514, doi:10.1029/93GL00367.

Andrews, D. J. (2002), A fault constitutive relation accounting for thermal pressurization of pore fluid, *J. Geophys. Res.*, *107*(B12), 2363, doi:10.1029/2002JB001942.

Beeler, N. M., T. E. Tullis, and J. D. Weeks (1994), The roles of time and displacement in the evolution effect in rock friction, *Geophys. Res. Lett.*, *21*, 1987–1990, doi:10.1029/94GL01599.

Beeler, N. M., T. E. Tullis, and D. L. Goldsby (2008), Constitutive relationship and physical basis of fault strength due to flash heating, *J. Geophys. Res.*, *113*, B01401, doi:10.1029/2007JB004988.

Bizzarri, A. (2009), Can flash heating of asperity contacts prevent melting?, *Geophys. Res. Lett.*, *36*, L11304, doi:10.1029/2009GL037335.

Bizzarri, A. (2010a), How to promote earthquake ruptures: Different nucleation strategies in a dynamic model with slip–weakening friction, *Bull. Seismol. Soc. Am.*, *100*(3), 923–940, doi:10.1785/0120090179.

Bizzarri, A. (2010b), An efficient mechanism to avert frictional melts during seismic ruptures, *Earth Planet. Sci. Lett.*, *296*, 144–152, doi:10.1016/j.epsl.2010.05.012.

Bizzarri, A. (2010c), Pulse-like dynamic earthquake rupture propagation under rate-, state- and temperature-dependent friction, *Geophys. Res. Lett.*, *37*, L18307, doi:10.1029/2010GL044541.

Bizzarri, A. (2010d), On the relations between fracture energy and physical observables in dynamic earthquake models, *J. Geophys. Res.*, *115*, B10307, doi:10.1029/2009JB007027.

Bizzarri, A. (2010e), On the recurrence of earthquakes: Role of wear in brittle faulting, *Geophys. Res. Lett.*, *37*, L20315, doi:10.1029/2010GL045480.

Bizzarri, A. (2011a), Dynamic seismic ruptures on melting fault zones, *J. Geophys. Res.*, *116*, B02310, doi:10.1029/2010JB007724.

Bizzarri, A. (2011b), On the deterministic description of earthquakes, *Rev. Geophys.*, *49*, RG3002, doi:10.1029/2011RG000356.

Bizzarri, A., and M. Cocco (2003), Slip-weakening behavior during the propagation of dynamic ruptures obeying rate- and state-dependent friction laws, *J. Geophys. Res.*, *108*(B8), 2373, doi:10.1029/2002JB002198.

Bizzarri, A., and M. Cocco (2005), 3D dynamic simulations of spontaneous rupture propagation governed by different constitutive laws with rake rotation allowed, *Ann. Geophys.*, *48*(2), 279–299.

Bizzarri, A., and M. Cocco (2006), A thermal pressurization model for the spontaneous dynamic rupture propagation on a three-dimensional fault: 2. Traction evolution and dynamic parameters, *J. Geophys. Res.*, *111*, B05304, doi:10.1029/2005JB003864.

Bizzarri, A., and P. Spudich (2008), Effects of supershear rupture speed on the high-frequency content of *S* waves investigated using spontaneous dynamic rupture models and isochrone theory, *J. Geophys. Res.*, *113*, B05304, doi:10.1029/2007JB005146.

Bizzarri, A., M. Cocco, D. J. Andrews, and E. Boschi (2001), Solving the dynamic rupture problem with different numerical approaches and constitutive laws, *Geophys. J. Int.*, *144*, 656–678, doi:10.1046/j.1365-246x.2001.01363.x.

Brantut, N., A. Schubnel, J. N. Rouzaud, F. Brunet, and T. Shimamoto (2008), High-velocity frictional properties of a clay bearing fault gouge and implications for earthquake mechanics, *J. Geophys. Res.*, *113*, B10401, doi:10.1029/2007JB005551.

Brantut, N., A. Schubnel, J. Corvisier, and J. Sarout (2010), Thermochemical pressurization of faults during cosesimic slip, *J. Geophys. Res.*, *115*, B05314, doi:10.1029/2009JB006533.

Brodsky, E. E., and H. Kanamori (2001), Elastohydrodynamic lubrication of faults, *J. Geophys. Res.*, *106*(B8), 16,357–16,374, doi:10.1029/2001JB000430.

Brune, J. N., S. Brown, and P. A. Johnson (1993), Rupture mechanism and interface separation in foam rubber models of earthquakes: A possible solution to the heat flow paradox and the paradox of large overthrusts, *Tectonophysics*, *218*, 59–67, doi:10.1016/0040-1951(93)90259-M.

Bureau, L., T. Baumberger, and C. Caroli (2000), Shear response of a frictional interface to a normal load modulation, *Phys. Rev. E*, *62*, 6810–6820, doi:10.1103/PhysRevE.62.6810.

Cochard, A., and R. Madariaga (1994), Dynamic faulting under rate–dependent friction, *Pure Appl. Geophys.*, *142*(3–4), 419–445, doi:10.1007/BF00876049.

Copley, A., J.-P. Avouac, J. Hollingsworth, and S. Leprince (2011), The 2001 M_w 7.6 Bhuj earthquake, low fault friction, and the crustal support of plate driving forces in India, *J. Geophys. Res.*, *116*, B08405, doi:10.1029/2010JB008137.

Day, S. M., L. A. Dalguer, N. Lapusta, and Y. Liu (2005), Comparison of finite difference and boundary integral solutions to three–dimensional spontaneous rupture, *J. Geophys. Res.*, *110*, B12307, doi:10.1029/2005JB003813.

De Paola, N., T. Hirose, T. Mitchell, G. Di Toro, T. Togo, and T. Shimamoto (2011), Fault lubrication and earthquake propagation in thermally unstable rocks, *Geology*, *39*, 35–38, doi:10.1130/G31398.1.

Dieterich, J. H. (1972), Time-dependent friction in rocks, *J. Geophys. Res.*, *77*, 3690–3697, doi:10.1029/JB077i020p03690.

Di Toro, G., R. Han, T. Hirose, N. De Paola, S. Nielsen, K. Mizoguchi, F. Ferri, M. Cocco, and T. Shimamoto (2011), Fault lubrication during earthquakes, *Nature*, *471*, 494–498, doi:10.1038/nature09838.

Dunham, E. M. (2007), Conditions governing the occurrence of supershear ruptures under slip–weakening friction, *J. Geophys. Res.*, *112*, B07302, doi:10.1029/2006JB004717.

Goldsby, D. L., and T. E. Tullis (2002), Low frictional strength of quartz rocks at subseismic slip rates, *Geophys. Res. Lett.*, *29*(17), 1844, doi:10.1029/2002GL015240.

Great Britain Department of Education and Science (1966), *Lubrication (Tribology)*, H. M. Stn. Off., London.

Guth, E., and R. Simha (1936), Untersuchungen über die viscosität von vuspensionen und lösungen. 3. Über die viskosität von kugelsuspensionen (in Deutch), *Kolloid Z.*, *74*, 266.

Han, R., T. Shimamoto, T. Hirose, J.-H. Ree, and J.-I. Ando (2007), Ultralow friction of carbonate faults caused by thermal decomposition, *Science*, *316*, 878–881, doi:10.1126/science.1139763.

Han, R., H. Hirose, and T. Shimamoto (2010), Strong velocity weakening and powder lubrication of simulated carbonate faults at seismic slip rates, *J. Geophys. Res.*, *115*, B03412, doi:10.1029/2008JB006136.

Han, R., T. Hirose, T. Shimamoto, Y. Lee, and J.-i. Ando (2011), Granular nanoparticles lubricate faults during seismic slip, *Geology*, *39*, 599–602, doi:10.1130/G31842.1.

Hanks, T. C. (1977), Earthquake stress drops, ambient tectonic stresses and stresses that drive plate motions, *Pure Appl. Geophys.*, *115*, 441–458, doi:10.1007/BF01637120.

Hirose, T., and M. Bystricky (2007), Extreme dynamic weakening of faults during dehydration by coseismic shear heating, *Geophys. Res. Lett.*, *34*, L14311, doi:10.1029/2007GL030049.

Hirose, T., and T. Shimamoto (2005), Growth of molten zone as a mechanism of slip weakening of simulated faults in gabbro during frictional melting, *J. Geophys. Res.*, *110*, B05202, doi:10.1029/2004JB003207.

Hull, J. (1988), Thickness-displacement relationships for deformation zones, *J. Struct. Geol.*, *10*, 431–435, doi:10.1016/0191-8141(88)90020-X.

Ida, Y. (1972), Cohesive force across the tip of a longitudinal-shear crack and Griffith's specific surface energy, *J. Geophys. Res.*, *77*(20), 3796–3805, doi:10.1029/JB077i020p03796.

Ikeda, R., Y. Iio, and K. Omura (2001), In situ stress measurements in NIED boreholes in and around the fault zone near the 1995 Hyogo-ken Nanbu earthquake, Japan, *Isl. Arc*, *10*, 252–260, doi:10.1046/j.1440-1738.2001.00323.x.

Ionescu, I. R., and M. Campillo (1999), Influence of the shape of the friction law and fault finiteness on the duration of initiation, *J. Geophys. Res.*, *104*(B2), 3013–3024, doi:10.1029/1998JB900090.

Jaeger, J. C., and N. G. W. Cook (1979), *Fundamentals of Rock Mechanics*, 591 pp., Chapman and Hall, London, doi:10.1017/CBO9780511735349.

Jeffreys, H. (1942), On the mechanics of faulting, *Geol. Mag.*, *79*, 291–295, doi:10.1017/S0016756800076019.

Kanamori, H., and D. L. Anderson (1975), Theoretical basis of some empirical relations in seismology, *Bull. Seismol. Soc. Am.*, *65*, 1073–1095.

Kanamori, H., J. Mori, and T. H. Heaton (1990), The 3 December 1988, Pasadena earthquake (M_L = 4.9) recorded with the very broadband system in Pasadena, *Bull. Seismol. Soc. Am.*, *80*, 483–487.

Karner, S. L., and C. J. Marone (1998), The effect of shear load on frictional healing in simulated fault gouge, *Geophys. Res. Lett.*, *25*, 4561–4564, doi:10.1029/1998GL900182.

Karner, S. L., C. J. Marone, and B. Evans (1997), Laboratory study of fault healing and lithification in simulated fault gouge under hydrothermal conditions, *Tectonophysics*, *277*, 41–55, doi:10.1016/S0040-1951(97)00077-2.

Koizumi, Y., K. Otsuki, A. Takeuchi, and H. Nagahama (2004), Frictional melting can terminate seismic slips: Experimental results of stick–slip, *Geophys. Res. Lett.*, *31*, L21605, doi:10.1029/2004GL020642.

Lachenbruch, A. H. (1980), Frictional heating, fluid pressure, and the resistance to fault motion, *J. Geophys. Res.*, *85*(B11), 6097–6112, doi:10.1029/JB085iB11p06097.

Lachenbruch, A. H., and J. H. Sass (1980), Heat flow and energetics of the San Andreas fault zone, *J. Geophys. Res.*, *85*(NB11), 6185–6222, doi:10.1029/JB085iB11p06185.

Linker, M. F., and J. H. Dieterich (1992), E1ects of variable normal stress on rock friction: Observations and constitutive equations, *J. Geophys. Res.*, *97*, 4923–4940, doi:10.1029/92JB00017.

Lockner, D. A., and N. M. Beeler (2002), Rock failure and earthquakes, in *Earthquake & Engineering Seismology*, edited by W. H. Lee et al., pp. 505–537, Academic, Amsterdam, doi:10.1016/S0074-6142(02)80235-2.

Ma, K.-F., E. E. Brodsky, J. Mori, C. Ji, T.-R. A. Song, and H. Kanamori (2003), Evidence for fault lubrication during the 1999 Chi–Chi, Taiwan, earthquake (Mw 7.6), *Geophys. Res. Lett.*, *30*(5), 1244, doi:10.1029/2002GL015380.

Madariaga, R., and A. Cochard (1994), Seismic source dynamics, heterogeneity and friction, *Ann. Geofis.*, *37*(6), 1349–1375.

Major, J. J., and T. C. Pierson (1992), Debris flow rheology: Experimental analysis of fine-grained slurries, *Water Resour. Res.*, *28*, 841–857, doi:10.1029/91WR02834.

Marone, C. J. (1998), The effect of loading rate on static friction and the rate of fault healing during the earthquake cycle, *Nature*, *391*, 69–72, doi:10.1038/34157.

Marrett, R., and R. W. Allmendinger (1990), Kinematic analysis of fault-slip data, *J. Struct. Geol.*, *12*, 973–986, doi:10.1016/0191-8141(90)90093-E.

Mase, C. W., and L. Smith (1987), Effects of frictional heating on the thermal, hydrological, and mechanical response of a fault, *J. Geophys. Res.*, *92*, 6249–6272, doi:10.1029/JB092iB07p06249.

Matsu'ura, M., H. Kataoka, and B. Shibazaki (1992), Slip-dependent friction law and nucleation processes in earthquake rupture, *Tectonophysics*, *211*, 135–148, doi:10.1016/0040-1951(92)90056-C.

Melosh, J. (1996), Dynamic weakening of faults by acoustic fluidization, *Nature*, *379*, 601–606, doi:10.1038/379601a0.

Mikumo, T., K. B. Olsen, E. Fukuyama, and Y. Yagi (2003), Stress-breakdown time and slip-weakening distance inferred from slip-velocity functions on earthquake faults, *Bull. Seismol. Soc. Am.*, *93*, 264–282, doi:10.1785/0120020082.

Mizoguchi, K., T. Hirose, T. Shimamoto, and E. Fukuyama (2007), Reconstruction of seismic faulting by high-velocity friction experiments: An example of the 1995 Kobe earthquake, *Geophys. Res. Lett.*, *34*, L01308, doi:10.1029/2006GL027931.

Mizoguchi, K., T. Hirose, T. Shimamoto, and E. Fukuyama (2009), Fault heals rapidly after dynamic weakening, *Bull. Seismol. Soc. Am.*, *99*(6), 3470–3474, doi:10.1785/0120080325.

Nadeau, R. M., and L. R. Johnson (1998), Seismological studies at Parkfield VI: Moment release rates and estimates of source parameters for small repeating earthquakes, *Bull. Seismol. Soc. Am.*, *88*, 790–814.

Noda, H., E. M. Dunham, and J. R. Rice (2009), Earthquake ruptures with thermal weakening and the operation of major faults at low overall stress levels, *J. Geophys. Res.*, *114*, B07302, doi:10.1029/2008JB006143.

Ohnaka, M. (2003), A constitutive scaling law and a unified comprehension for frictional slip failure, shear fracture of intact rocks, and earthquake rupture, *J. Geophys. Res.*, *108*(B2), 2080, doi:10.1029/2000JB000123.

Power, W. L., and T. E. Tullis (1991), Euclidean and fractal models for the description of rock surface roughness, *J. Geophys. Res.*, *96*, 415–424, doi:10.1029/90JB02107.

Power, W. L., T. E. Tullis, and D. J. Weeks (1988), Roughness and wear during brittle faulting, *J. Geophys. Res.*, *93*(B12), 15,268–15,278, doi:10.1029/JB093iB12p15268.

Prakash, V. (1998), Frictional response of sliding interfaces subjected to time varying normal pressures, *J. Tribol.*, *120*, 97–102, doi:10.1115/1.2834197.

Prakash, V., and R. J. Clifton (1992), Pressure–shear plate impact measurement of dynamic friction for high speed machining applications, paper presented at Seventh International Congress on Experimental Mechanics, Soc. of Exper. Mech., Bethel, Conn.

Prakash, V., and F. Yuan (2004), Results of a pilot study to investigate the feasibility of using new experimental techniques to measure sliding resistance at seismic slip rates, *Eos Trans. AGU*, *85*(47), Fall Meet. Suppl., Abstract T21D-02.

Rathbun, A. P., and C. J. Marone (2010), Effect of strain localization on frictional behavior of sheared granular materials, *J. Geophys. Res.*, *115*, B01204, doi:10.1029/2009JB006466.

Reches, Z., and D. A. Lockner (2010), Fault weakening and earthquake instability by powder lubrication, *Nature*, *467*, 452–455, doi:10.1038/nature09348.

Rice, J. R. (2006), Heating and weakening of faults during earthquake slip, *J. Geophys. Res.*, *111*, B05311, doi:10.1029/2005JB004006.

Rice, J. R., N. Lapusta, and K. Ranjith (2001), Rate and state dependent friction and the stability of sliding between elastically deformable solids, *J. Mech. Phys. Solids*, *49*, 1865–1898, doi:10.1016/S0022-5096(01)00042-4.

Richardson, E., and C. J. Marone (1999), E1ects of normal force vibrations on frictional healing, *J. Geophys. Res.*, *104*, 28,859–28,878, doi:10.1029/1999JB900320.

Ruina, A. L. (1983), Slip instability and state variable friction laws, *J. Geophys. Res.*, *88*(B12), 10,359–10,370, doi:10.1029/JB088iB12p10359.

Scholz, C. H. (2002), *The Mechanics of Earthquakes and Faulting*, 2nd ed., 439 pp., Cambridge Univ. Press, New York.

Segall, P., and J. R. Rice (2006), Does shear heating of pore fluid contribute to earthquake nucleation?, *J. Geophys. Res.*, *111*, B09316, doi:10.1029/2005JB004129.

Sibson, R. H. (1974), Frictional constraints on thrust, wrench, and normal faults, *Nature*, *249*, 542–544, doi:10.1038/249542a0.

Sibson, R. H. (1975), Generation of pseudotachylyte by ancient seismic faulting, *Geophys. J. R. Astron. Soc.*, *43*, 775–794, doi:10.1111/j.1365-246X.1975.tb06195.x.

Sommerfeld, A. (1950), *Mechanics of Deformable Bodies*, Elsevier, New York.

Sone, H., and T. Shimamoto (2009), Frictional resistance of faults during accelerating and decelerating earthquake slip, *Nat. Geosci.*, *2*, 705–708, doi:10.1038/ngeo637.

Spikes, H. A. (1997), Mixed lubrication—An overview, *Lubric. Sci.*, *9*(3), 221–253, doi:10.1002/ls.3010090302.

Spray, J. G. (1993), Viscosity determinations of some frictionally generated silicate melts: Implications for fault zone rheology at high strain rates, *J. Geophys. Res.*, *98*, 8053–8068, doi:10.1029/93JB00020.

Suppe, J. (2007), Absolute fault and crustal strength from wedge tapers, *Geology*, *35*, 1127–1130, doi:10.1130/G24053A.1.

Szeri, A. Z. (2011), *Fluid Film Lubrication*, 2nd ed., 547 pp., Cambridge Univ. Press, New York.

Tinti, E., A. Bizzarri, A. Piatanesi, and M. Cocco (2004), Estimates of slip weakening distance for different dynamic rupture models, *Geophys. Res. Lett.*, *31*, L02611, doi:10.1029/2003GL018811.

Tsutsumi, A., and T. Shimamoto (1997), High velocity frictional properties of gabbro, *Geophys. Res. Lett.*, *24*, 699–702, doi:10.1029/97GL00503.

Tullis, T. E., and D. L. Goldsby (2003a), Flash melting of crustal rocks at almost seismic slip rates, *Eos Trans. AGU*, *84*(46), Fall Meet. Suppl., Abstract S51B-05.

Tullis, T. E., and D. L. Goldsby (2003b), Laboratory experiments on fault shear resistance relevant to coseismic earthquake slip, report, South. Calif. Earthquake Cent., Los Angeles.

Vavryčuk, V. (2011), Tensile earthquakes: Theory, modeling, and inversion, *J. Geophys. Res.*, *116*, B12320, doi:10.1029/2011JB008770.

Wald, D. J. (1992), Strong motion and broadband teleseismic analysis of the 1991 Sierra Madre, California, earthquake, *J. Geophys. Res.*, *97*, 11,033–11,046, doi:10.1029/92JB00565.

Wibberley, C. A. J., and T. Shimamoto (2005), Earthquake slip weakening and asperities explained by thermal pressurization, *Nature*, *436*, 689–692, doi:10.1038/nature03901.

Wu, F. T., L. Blatter, and H. Roberson (1975), Clay gouges in the San Andreas Fault System and their possible implications, *Pure Appl. Geophys.*, *113*, 87–95, doi:10.1007/BF01592901.

Yamamoto, K., and Y. Yabe (2001), Stresses at sites close to the Nojima Fault measured from core samples, *Isl. Arc*, *10*, 266–281, doi:10.1046/j.1440-1738.2001.00325.x.

Yamashita, T. (2000), Generation of microcracks by dynamic shear rupture and its effects on rupture growth and elastic wave radiation, *Geophys. J. Int.*, *143*, 395–406, doi:10.1046/j.1365-246X.2000.01238.x.

Zolotarev, N. V., L. I. Vysotskii, and V. M. Dorodnov (1966), Determining the viscosity of grinding slurry in relation to concentration of fine abrasive, *Glass Ceram.*, *23*, 519–522, doi:10.1007/BF00678922.